View metadata, citation and similar papers at core.ac.uk

brought to you by CORE

provided by ScholarWorks@UNIST

COMMONS DEED

저작자표시-변경금지 2.0 대한민국

이용자는 아래의 조건을 따르는 경우에 한하여 자유롭게

- 이 저작물을 복제, 배포, 전송, 전시, 공연 및 방송할 수 있습니다.
- 이 저작물을 영리 목적으로 이용할 수 있습니다.

다음과 같은 조건을 따라야 합니다:

저작자표시. 귀하는 원저작자를 표시하여야 합니다.

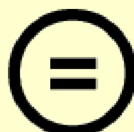

변경금지. 귀하는 이 저작물을 개작, 변형 또는 가공할 수 없습니다.

- 귀하는, 이 저작물의 재이용이나 배포의 경우, 이 저작물에 적용된 이용허락조건을 명확하게 나타내어야 합니다.
- 저작권자로부터 별도의 허가를 받으면 이러한 조건들은 적용되지 않습니다.

저작권법에 따른 이용자의 권리는 위의 내용에 의하여 영향을 받지 않습니다.

이것은 이용허락규약(Legal Code)을 이해하기 쉽게 요약한 것입니다.

Disclaimer

ULSAN NATIONAL INSTITUTE OF
SCIENCE AND TECHNOLOGY

A Study on SPICE Modeling of Non-Resonant Plasmonic Terahertz Detector

JeongSeop Lee

School of Electrical and Computer Engineering

Electrical Engineering Program

Graduate school of UNIST

UNIST
ULSAN NATIONAL INSTITUTE OF
SCIENCE AND TECHNOLOGY

A Study on SPICE Modeling of Non-Resonant Plasmonic Terahertz Detector

A thesis
Submitted to the Graduate School of UNIST
in partial fulfillment of the
requirements for the degree of
Master of science

Jeongseop Lee

12. 19. 2014 of submission

Approved by

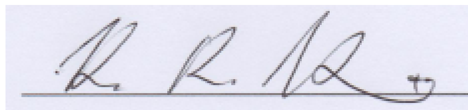

Major Advisor
Kyung Rok Kim

ULSAN NATIONAL INSTITUTE OF
SCIENCE AND TECHNOLOGY

A Study on SPICE Modeling of Non-Resonant Plasmonic Terahertz Detector

Jeongseop Lee

This certifies that the thesis of Jeongseop Lee is approved.

12. 19. 2014 of submission

Signature

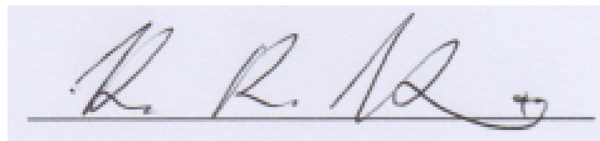

Thesis Supervisor: Kyung Rok Kim

Signature

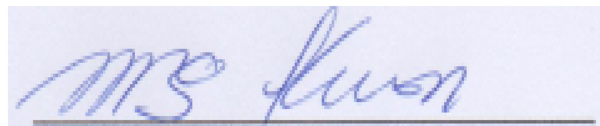

Typed name: Min-Suk Kwon

Signature

Typed name: Youngmin Kim

ULSAN NATIONAL INSTITUTE OF SCIENCE AND TECHNOLOGY

Abstract

The terahertz (sub-millimeter wave) is the frequency resource, ranging from 100 GHz ~ 10 THz band, located in the middle region of the infrared and millimeter waves in the electromagnetic spectrum. Terahertz waves has unique physical characteristics, which is transparency of radio waves and straightness of light waves, simultaneously. The terahertz wave is applied to the basic science, such as device, spectroscopy, and imaging technology. And also adjust in the applied science, such as biomedical engineering, security, environment, information and communication. Which importance already verified. In the new shape of future market is expected to be formed broadly. For this application, operating in the THz frequency detecting device essential. Recently, Current elements operating in terahertz are presented, such as compound semiconductor (Ⅲ-ⅤHBT, HEMT). But, there are disadvantage to use as a high price. Therefore, research have been made of silicon based THz detector in many research groups. Silicon-based nano-technology utilizes a plasma wave transistor technology. Which is using the space-time change of the channel charge density. That causes plasma wave oscillation in the MOSFET (Metal oxide semiconductor field effect transistor) channel and this effect available MOSET operating terahertz regime beyond MOSFET cut-off frequency. So, PWT (plasma wave transistor) is available terahertz detection and oscillation. For integrated possible post processing circuit development in these of terahertz applications system, silicon based PWT compact model is essential thing. For this compact model for spice simulation beyond cut-off frequency, we consider charge time variance model which is NQS (non-quasi-static) model, not quasi-static model. For NQS model two kinds of model exist, first is RC ladder model. That is seral connect MOSFET get rid of parasitic elements. And these complex circuit making the equivalent circuit model, it called New Elmore model. For post processing circuit simulation, fast simulation speed is essential, RC ladder model has a disadvantage (for simulating each segment). In this thesis we using New Elmore model based on Non-resonant plasmonic THz detector modeling, And verified physical validity of our NQS model using the our TCAD model based on Quasi-plasma 2DEG. And we propose fast and accurate compact modeling

ULSAN NATIONAL INSTITUTE OF SCIENCE AND TECHNOLOGY

Contents

I. Introduction ……………………………………………………………………………1

1.1 Terahertz and Application………………..1

1.2 Terahertz Detector …………………………………………………………………....2

1.2.1 Plasma Wave FET Theory……………………………..…………………2

1.2.2 Terahertz Detector Operating Principle……………………...……………….5

1.3 Motivation ……………………………………………………………………………10

1.4 Thesis Overview……………………………………………………………………10

II. Modeling and Simulation of Terahertz Detector…...…………………………….……12

2.1 Modeling Terahertz Detector……………………………………………….....…12

2.1.1 Quasi Static, Non Quasi Static..…………………………...……………12

2.1.2 TCAD Modeling (Boundary Condition)…………………….………………15

2.1.3 Quasi Plasma 2DEG …………………………...………………………...16

2.1.4 SPICE Modeling (Boundary Condition)……………………………………..18

2.1.5 SPICE Modeling (Non Quasi Static)…………………………………...…19

2.2 Simulation Results of Terahertz Detector……………………………………………21

2.2.1 TCAD,SPICE Simulation Results……………………………………….....21

2.2.2 Physical Validity of NQS model…… …………....………………………….23

2.2.3 Noise Equivalent Power…………………………………………………..25

III. Summary & Conclusion ……………………..……………………………………….27

IV. Future Works ……………………………………………………………………28

ULSAN NATIONAL INSTITUTE OF
SCIENCE AND TECHNOLOGY

List of Figures

Figure 1-1. The electromagnetic spectrum

Figure 1-2. Terahertz technology application (a) imaging- 2D image of human tooth, (b) spectroscopy – tablet spectroscopy (c) communication – wideband communication in broadcasting

Figure 1-3. Comparison of plasma and transit mode operating frequency limits vs. gate length for several semiconductor materials.

Figure 1-4. Plasma oscillations in FET channel ungated 2DEG, gated 2DEG

Figure 1-5. Schematics of a FET as a THz detector (a) and the equivalent circuit resonant detector (b), non-resonant detector(c) [1]

Figure 1-6. Terahertz operation principle (a) resonant detector, (c) resistive mixer, (b), (d) non resonant detector

Figure 2-1. Terahertz detector structure and simulation framework based on Si FET. To the boundary condition external capacitor connected to gate and drain

Figure 2-2. Contour plot of the channel electron density modulation along with the channel position at the same gate overdrive voltage V_g-V_{th}= 0.1 and each gate incident frequency (a) 6 GHz, (b) 60 GHz, (c) 600 GHz

Figure 2-3. Calculation of the plasma wave transit time, oscillation period

Figure 2-4. The applied asymmetric boundary condition in the transient simulation of the mixed-mode TCAD framework (Fig. 2-1) by adding varied external capacitance between gate and drain

Figure 2-5. Contour plots of the channel electron density modulation along with the channel position at each time scale. The 2DEG density is modulated near source side due to incoming THz radiation with f=0.7THz (a) symmetry condition, (b) C_{gd}= 1 pF

ULSAN NATIONAL INSTITUTE OF SCIENCE AND TECHNOLOGY

Figure 2-6. Contour plots of the channel density modulation along with the channel position

Figure 2-7. Si MOSFET-based THz detector structure and circuit configuration in TCAD simulation, Inset shows the quasi-plasma electron box as 2DEG in the channel region

Figure 2-8. The schematic of applied asymmetric boundary condition in the transient simulation of the mixed-mode SPICE framework by adding varied external capacitance between gate and drain (L_g= 300 nm, t_{ox}= 1.1nm, V_{th}= 0.2V)

Figure 2-9. The applied asymmetric boundary condition in the transient simulation of the mixed-mode SPICE framework (Fig. 2-1) by adding varied external capacitance between gate and drain

Figure 2-10. Equivalent circuit of the NQS model [43]

Figure 2-11. Equivalent circuit BSIM model (a) quasi-static model, (b) new Elmore equivalent model for non quasi static model [42]

Figure 2-12. Simulation results of photoresponse in TCAD framework as a function of a gate voltage (a) Without Quasi plasma 2DEG, (b) Apply Quasi plasma 2DEG in the channel

Figure 2-13. Schematic of simulation circuit, NMOS L_g= 300nm, t_{ox}= 1.1 nm, V_{th}= 0.2

Figure 2-14. Transient simulation results of drain voltage each gate DC voltage 0, 0.1, -0.2V respectively

Figure 2-15. SPICE simulation results of the photoresponse by function of gate voltage (a) Quasi static model, (b) Non Quasi static model

Figure 2-16. Contour plots of the channel density modulation along with the channel position at the same gate overdrive voltage V_g-V_{th}

ULSAN NATIONAL INSTITUTE OF
SCIENCE AND TECHNOLOGY

Figure 2-17. Contour plots of the channel density modulation along with the channel position at the same gate overdrive voltage V_g - V_{th}

Figure 2-18. The simulation results as a function of gate voltage according to the variation t_{ox} (=1.1, 2.5, and 4 nm) spice simulation results (right).

Figure 2-19. Simulation results of the SPICE photoresponse peak value of at each gate length

Figure 2-20. SPICE simulation results of photoresponse peak vary the gate to drain capacitance

Figure 2-21. Full protocol for determining R_v and NEP

Figure 4-1. Terahertz chip board

Figure 4-**2.** Block diagram of the terahertz chip board

ULSAN NATIONAL INSTITUTE OF
SCIENCE AND TECHNOLOGY

List of Tables

Table I. Calculation results of plasma wave transit time (L_g=300 nm), oscillation period of the each frequency (6 GHz, 7 GHz, 600 GHz, 700 GHz).

ULSAN NATIONAL INSTITUTE OF
SCIENCE AND TECHNOLOGY

Nomenclature

AC	Alternating current
BSIM	Berkeley short channel IFGET model
CMOS	Complementary metal oxide semiconductor
DC	Direct current
DFG	Difference frequency generation
EM	Electromagnetic
FET	Field effect transistor
FPA	Focal plane array
HBT	Heterojunction bipolar transistor
HD	High definition
HEMT	High electron mobility transistor
IC	Integrated circuit
LPF	Low pass filter
NMOS	N-channel metal oxide semiconductor
NQS	Non quasi static
PWT	Plasma wave transistor
QS	Quasi static
RF	Radio frequency
RTD	Resonant tunneling diode
SBD	Schottky barrier diode
Si	Silicon
SPICE	Simulation program with integrated circuit emphasis

ULSAN NATIONAL INSTITUTE OF
SCIENCE AND TECHNOLOGY

TCAD	Technology computer aided design
THz	Terahertz
THz QCL	Terahertz quantum cascade laser
UTC-PD	Uni-travelling carrier photodiode
2DEG	Two-dimensional electron gas
2D	Two-dimensional

ULSAN NATIONAL INSTITUTE OF SCIENCE AND TECHNOLOGY

Chapter 1

Introduction

1.1 Terahertz and application

Terahertz is the frequency resource ranging from 100 GHz to 10 THz band, wave length is 0.1 mm to 1 mm (sub-millimeter wave) located in the middle region of the electromagnetic wave and infrared wave in the electromagnetic spectrum (Fig 1-1). Which is shortest wave length electromagnetic (EM) wave has special characteristic. Terahertz wave has straightness of light wave and transparency of radio waves simultaneously, for this region terahertz wave advantage in diversified technical application. Field research was done less than in other frequency bands, it is called “terahertz gap” in the sense that empty frequency band.

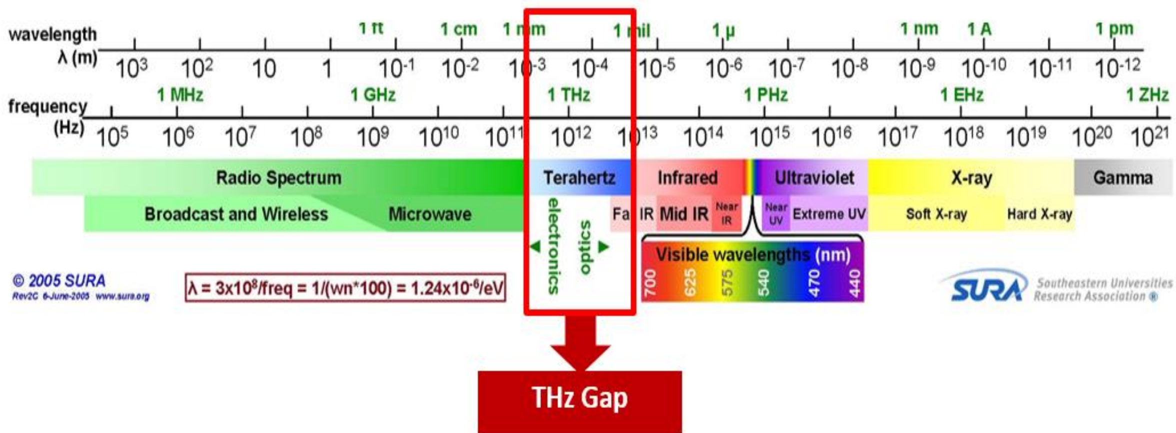

Figure 1-1. The electromagnetic spectrum

Research of terahertz technology, research was done in the optical field primarily. But, nano electronic devices and materials technology development gradually. Which is being deployed as an aspect of mixed optical engineering and electronic engineering. Optical technology as photoconductive switch, optical rectification, difference frequency generator (DFG), optical parametric, terahertz quantum cascade laser (THz QCL), and uni-travelling carrier photodiode (UTC-PD) are developed. As a side electronic engineering part Schottky barrier diode (SBD), resonant tunneling diode (RTD), like passive elements research n actively underway. Heterojunction bipolar transistor (HBT), high electron mobility transistor (HEMT) [1]-[11], silicon semiconductor [29]-[32] device has enable to sub THz operation. For nano device process technology for high cutoff frequency, scaled down to 20 nm. Gate length reduction in transit mode there is the operation limit up to 0.5 THz. In order to overcome operating THz regime, utilizing plasma wave transistor (PWT) [12][13] using a plasma wave which is

ULSAN NATIONAL INSTITUTE OF SCIENCE AND TECHNOLOGY

defined wave space, time variation of the channel electron density. It is able to operate at 10 to 100 times the speed of transit-mode electron drift velocity [12][13]. Using the plasma resonance phenomenon of 2D channel electron density, operating in a high frequency region which is able to cutoff frequency of the transistor. Application of terahertz technology divided into three fields, imaging, spectroscopy, and wireless communication has been active in the field of research. Imaging part is applied biomedical (Fig. 1-2(a)) [22], and security field. Spectroscopy field is using in nondestructive inspection in industries (Fig. 1-2(b)) [23]. Wireless communication [24][25] is applied transmission of uncompressed HD television broadcasting in 0.1THz regime [26]-[28].

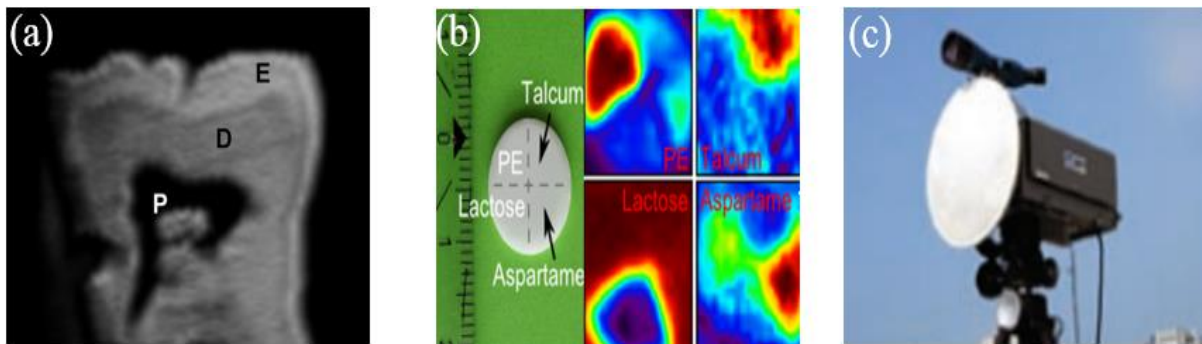

Figure 1-2. Terahertz technology application (a) imaging- 2D image of human tooth, (b) spectroscopy – tablet spectroscopy (c) communication – wideband communication in broadcasting

1.2 Terahertz detector

High speed and ultra-high frequency performance enhancement of existing nano electronic device is settled transit mode operation in whether electrons forming a channel how rapidly moves. Electron velocity in this region is limited by scattering in the solid crystal structure, a saturation speed of about 10^6 cm/sec, in scattering without the mean free path, in theory to reach the ballistic transport area that has a transfer speed of 10^7 cm/sec. Figure 1-3 determined by the cut-off frequency electronic drift velocity of electrons elements operating in transit mode, transistors with the scaled down in nanometers, transit time of the electrons is to be smaller than the electron momentum relaxation time, τ_m would be accessed ballistic area. Plasma wave velocity in the channel of the field effect transistor (FET) , when the transit time is decrease by being several hundred times higher than the electron drift velocity, $\omega_p\tau_m$ > 1 state satisfies a much easier $2\pi\tau_m/t_{tr}$ > 1 condition. t_{tr} is the electron momentum relaxation time. Satisfy this condition $\omega_p\tau_m$ > 1, FET operates as a plasma wave resonator. Fundamental frequency of the resonator, detector are tuning by the gate bias[53], V_g THz band, not only mixer, as the signal source, can be utilized at much higher THz frequency range than existing transit mode operation

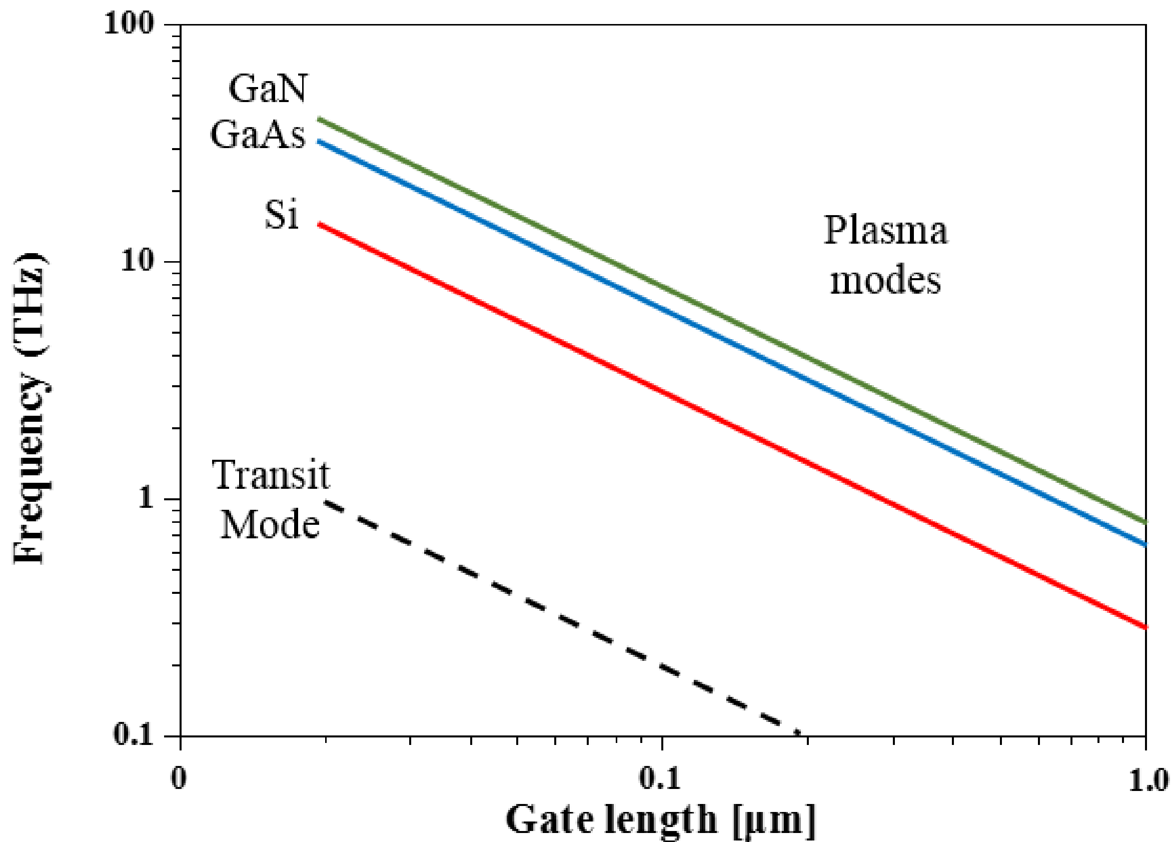

Figure 1-3. Comparison of plasma and transit mode operating frequency limits vs. gate length for several semiconductor materials.

1.2.1 Plasma wave transistor (PWT) theory

Related to the theory of plasma wave transistors, begins with M. Dyakonov, M. Shur [12][13]. In Fig. 1-4. The channel length is very short 2D electron gas (2DEG) under the transfer of electrons at the FET channel, can be expressed by hydrodynamic equation (Eq. 1.1), continuity equation (Eq. 1.2) rather than the movement of the particles, respectively electrons and a hydrodynamic wave equation shallow water interpreted to be similar[12].

$$\frac{\partial v}{\partial t} + v\frac{\partial v}{\partial x} + \frac{e}{m}\frac{\partial U}{\partial x} + \frac{v}{\tau} = 0 \tag{1.1}$$

$$\frac{\partial U}{\partial t} + \partial\frac{(Uv)}{\partial x} = 0 \tag{1.2}$$

ULSAN NATIONAL INSTITUTE OF SCIENCE AND TECHNOLOGY

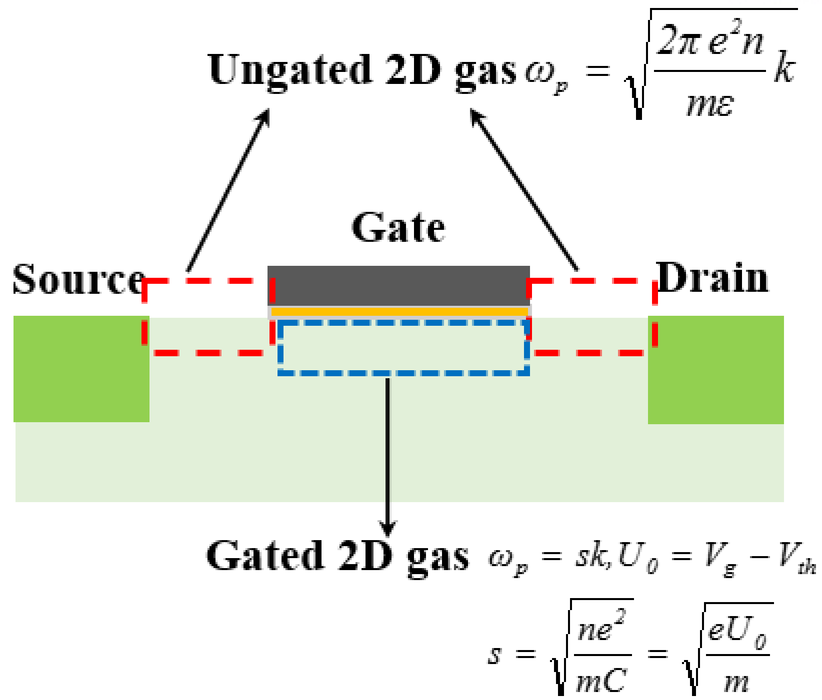

Figure 1-4. Plasma oscillations in FET channel un-gated 2DEG, gated 2DEG

The dispersion of plasma wave is $k = \omega_p/s$, k is the wave vector, ω_p is the frequency of plasma wave. Plasma wave velocity be proportional to electron carrier density of the channel, capacitance between gate and the channel. Which defined as[51]:

$$s = \frac{\sqrt{4\pi e^2 n}}{m\varepsilon} \tag{1.3}$$

In Eq. 1.3, e is electronic charge, n is the sheet electron density for channel region, m is electron effective mass, and dielectric constant ε. For electrons under the gate of a FET, the relation between the charge density and the electric field in the channel is readily obtained from the plane capacitor formula: [54]

$$en = CU \tag{1.4}$$

Where e, C, U is elementary charge, gate to channel capacitance per unit area, gate channel voltage respectively. Under static conditions and in the absence of the drain current, $U = U_0 = V_g - V_{th}$, where U_0 is the gate overdrive voltage, V_g is the gate voltage, V_{th} is the threshold voltage. Thus, PWT vary the channel electron density with the gate bias voltage. In this variation adjusting the resonant frequency selectively, which can be used as a frequency variable detection device. The plasma oscillation

frequency is determined by the geometric parameters of the channel electron density, channel length, source to drain region, and gate to drain region.

When satisfied with asymmetric boundary conditions between the source and drain (Eq. 1.5, 1.6) [16], Flow of the wave inside the channel is unstable, by amplification of the wave by continuous reflection between the source drain that occurs plasma wave oscillation.

$$U_g(0,t) = U_a sin\omega t + V_g \quad (1.5)$$

$$U_g(L,t) = V_g \quad (1.6)$$

In this case, the oscillation frequency of plasma wave as following Eq. 1.7:

$$\omega = (2p-1)\frac{\sqrt{eU_0/m}}{8\pi L} \quad (1.7)$$

L is the channel length of MOSFET, p is the integer, when p is 1 oscillation frequency is fundamental frequency. As a result, nanometer FET device is that operating THz detector device, detector operating frequency is tuned by gate bias voltage. And there is another important performance evaluation index ($\omega\tau$ = quality factor) to evaluate the plasma resonance. τ is the electron momentum relaxation time to determine the resonance characteristic spectral line width. $\omega\tau > 1$ regime, PWT FET operates resonant detector. $\omega\tau < 1$ regime plasma wave in the channel is over damping, operating non resonant detector[1].

1.2.2 Terahertz detector operating principle

To analyze the plasma wave nonlinear characteristic of at 2DEG channel for detection and mixing of the THz wave, and treat the plasma resonant and non-resonant operation range from dispersion transmission line. Generally the FET channel described as Fig. 1-5, resistor (R), capacitor(C), inductor (L) can be represented by equivalent circuit model. The equivalent circuit model gate to channel capacitance and channel resistance as the channel electron density by the gate voltage can be written as following Eq. 1.4. In Fig. 1-5(b) show that inductance role is kinetic inductance is proportional to the electron effective mass. Kinetic inductance serves as the electron inertia [35]. It operate by resonant THz detector. As shown in Fig. 1-5(c) channel equivalent circuit consist of resistor and capacitor without inductor, which do not serves as the electron inertia. It operate by non-resonant THz detector. Operates region of the PWT can be in two regions according to the operating frequency, and dependence of operation region on the gate length is shown in Fig. 1-6

ULSAN NATIONAL INSTITUTE OF SCIENCE AND TECHNOLOGY

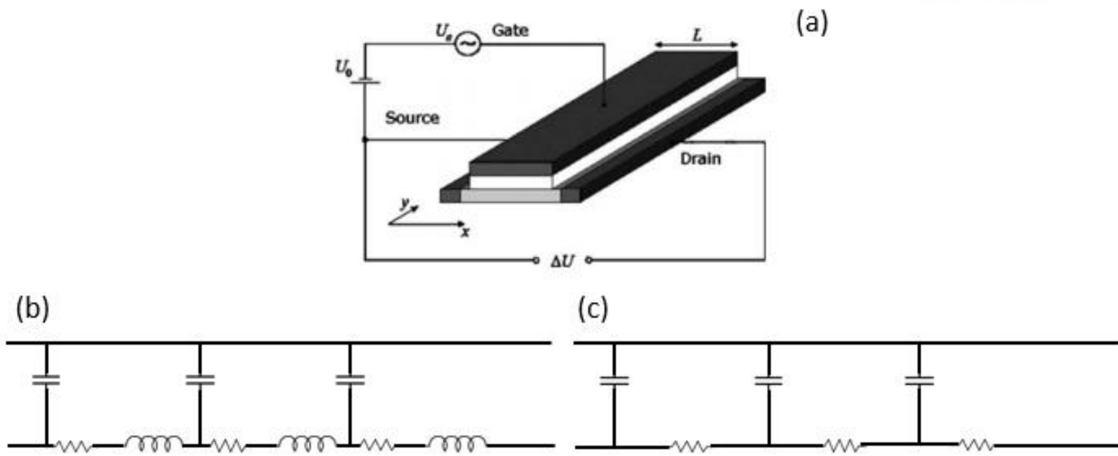

Figure 1-5. Schematics of a FET as a THz detector (a) and the equivalent circuit resonant detector (b), non-resonant detector(c) [1]

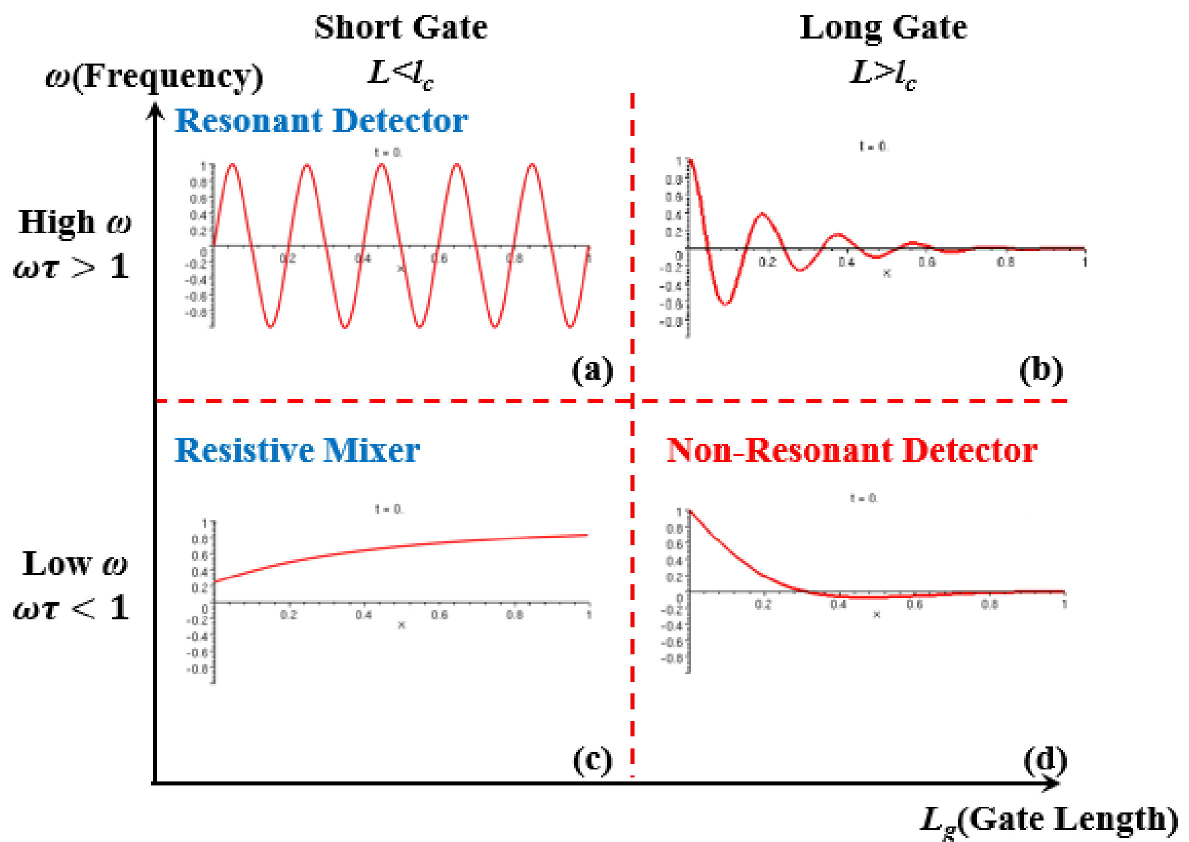

Figure 1-6. Terahertz operation principle (a) resonant detector, (b) non-resonant detector, (c) resistive mixer, (d) non resonant detector

1. High frequency regime occurs when $\omega\tau > 1$, that determines the conductivity ($\sigma = ne^2\tau/m$) of the channel. In this case, kinetic inductance of the Fig1-6(b) is a very important factor in determining the resonant mode. Plasma wave similar to the propagation of waves in the RLC transmission lines. Plasma waves decay time while τ would be to proceed with the wave speed of the equation:

$$s = \sqrt{\frac{ne^2}{mC}} = \sqrt{\frac{eU_0}{m}} \tag{1.8}$$

1-a. Resonant mode: short gate $L < s\tau$. In Fig 1-6(a) the plasma wave is repeatedly reflected at the boundary of the source and drain channel, forming a standing wave of large amplitude. At this time, the channel is to operate as a resonator for the plasma oscillation. The fundamental frequency of the plasma wave is $\sim s/L$

1-b. Long gate $L >> s\tau$. The plasma waves excited at the source will decay before reaching the drain, so that the ac current will exist only in a small part of the channel adjacent to the source.

2. Low frequency regime occurs when $\omega\tau < 1$, the plasma wave cannot exist because of an over damping at low frequency. This behavior is represented by RC circuit is the inductance is a simple short circuit in Fig. 1-5(c), therefore, the operating characteristics are determined by the gate length, denotes a time constant for $\omega\tau_{RC}$ by RC time constant. Here the resistance of the entire MOSFET channel is $L\rho/W$, the overall capacitance is CWL (W is the gate width, ρ is the channel resistance) the time constant is $\tau_{RC} = L^2\rho C$

2-a. Resistive mixer mode: Short gate, $L < (\rho C\omega)^{-1/2}$. $\omega\tau_{RC} < 1$, ac current is flow along the gate-channel capacitance over the whole length of the MOSFET gate. This operation method is called resistive mixer. The behavior takes place in a very short gate region in THz regime. For example, for the operation of 1 THz, the silicon MOSFET, it can be applied to 70 nm following PWT [16].

2-b Non resonant mod: Long gate $> (\rho C\omega)^{-1/2}$. $\omega\tau_{RC} >> 1$, The ac current is induced in the channel in the channel is much leakage at the gate cannot go from source. $l << L$ long gate device, Than from l more distance away from the source, there is no more ac current and ac voltage.

Finds the characteristic gate length distinguishing regimes 2-a, and 2-b is around 100nm [1]. If the conditions of the case 1-a are satisfied, the detector operate will be resonant, corresponding to the excitation of discrete plasma oscillation modes in the channel. Otherwise, the PWT will operate as a non-resonant (broadband) detector. Operation regime 1-b, 2-b, independently of the $\omega\tau$, if the ac current generated in the input signal cannot reach towards the drain, the output voltage can be simplified to the

following equation [13]:

$$\Delta U = \frac{U_a^2}{4U_0^2}\left[1 + \frac{2\omega\tau}{\sqrt{1+\omega\tau^2}}\right] \quad (1.9)$$

Equation (1.9) can be derived from the hydrodynamic equation (1.1) and continuity equation (1.2). On the basis of these physical consideration, focused on the design non-resonant THz detector. In FET, condition to operate detector mode asymmetry boundary condition (Eq. 1.5, 1.6) is applied. In the non-resonant case ($\omega\tau$ < 1), Eq 1.1 $\partial v/\partial t$ (kinetic inductance in Fig. 1-5(b)), $\partial v/\partial x$ terms can be neglected and rewritten as :

$$v = -\frac{e\tau}{m}\frac{\partial U}{\partial x} = -\mu\frac{\partial U}{\partial x} \quad (1.10)$$

Where electron mobility, $\mu = e\tau/m$,. For solving Eq. 1.1 and 1.2 apply that from:

$$v = v_0 + v_1 + v_2 \quad (1.11)$$

$$U = U_0 + U_1 + U_2 \quad (1.12)$$

Where v_0 is time averaged values of the electron velocity and U_0 is time averaged values of the channel potential, and v_n and U_n term is vary with time and the frequency $n\omega$, where ω is the incident frequency of the detector. In this case v_1, U_1 are proportional to U_a, while v_2 and U_2 are proportional to U_a^2. In the first order in U_a, using Eq. 1.1, 1.2 is rewritten and simplified as:

$$\frac{\partial U_1}{\partial t} + U_0 \cdot \left(\frac{-e\tau}{m}\right) \cdot \frac{\partial^2 U_1}{\partial x^2} = 0 \quad (1.13)$$

$$\frac{\partial U_1}{\partial t} = s^2\tau\frac{\partial^2 U_1}{\partial x^2} \quad (1.14)$$

where s is the plasma wave velocity can be defined as:

$$s = \sqrt{\frac{eU_0}{m}} \quad (1.15)$$

with the boundary conditions $U_1(x,t) = U_a cos\omega t, U_1(\infty,t) = 0$ the solution of Eq. 1.14 is given as:

ULSAN NATIONAL INSTITUTE OF
SCIENCE AND TECHNOLOGY

$$U_1(x,t) = U_a exp\left(- x/l\right)cos\left(\omega t - x/l\right) \quad (1.16)$$

where characteristic length l is the decay of the ac voltage away from source is defined as:

$$l = s\sqrt{\frac{2\tau}{\omega}} \quad (1.17)$$

In the second order in U_a, Eq. 1.2 is rewritten as:

$$\frac{\partial U_2}{\partial t} + \frac{\partial}{\partial x}(U_0 V_2 + U_1 v_1) = 0 \quad (1.17)$$

From this equation, using Eq. 1.10, each term of integrated results of are as follows:

$$\int_0^T \frac{\partial U_2}{\partial t} dt = U_2\left(T\right) - U_2\left(0\right) = 0 \quad (1.18)$$

$$\int_0^T U_0 v_2 dt = TU_0 v_2 = -\mu T U_2\left(\frac{\partial U_2}{\partial x}\right) \quad (1.19)$$

$$T \cdot \frac{1}{T}\int_0^T U_1 v_1 dt = T\left\langle U_1 v_1\right\rangle = -\mu T\left\langle U_1\left(\frac{\partial U_1}{\partial x}\right)\right\rangle \quad (1.20)$$

From the above integrated equations, Eq. 1.14 is rewritten as:

$$U_0 \frac{\partial U_2}{\partial x} + \left\langle U_1 \frac{\partial U_1}{\partial x}\right\rangle = 0 \quad (1.21)$$

angular brackets means the time average over one oscillation period ($T= 2\pi/\omega$). Eq. 1.11 means simply the absence of the DC current. An expression for the detector response ΔU is found by integrating Eq. 1.21:

$$U_2(x) = \frac{1}{2U_0}\left[\left\langle U_1^2(0,t)\right\rangle - \left\langle U_1^2(x,t)\right\rangle\right] \quad (1.22)$$

where the time averaged quantity is:

$$\left\langle U_1^2\left(x,t\right)\right\rangle = \left(1/2\right)U_a^2 exp\left(-2x/l\right) \quad (1.23)$$

found Eq. 1.16. Eq. 1.22 is rewritten and simplified as:

$$\Delta U = U_2(0) = \frac{U_a^2}{2U_0}\left[\frac{1}{2}U_a^2\right] = \frac{U_a^2}{4U_0} \tag{1.24}$$

$$U_2(x) = \frac{1}{2U_0}\left[\frac{1}{2}U_a^2 - \frac{1}{2}U_a^2 exp(-\frac{2x}{l})\right] \tag{1.25}$$

$$U_2(x) = \frac{U_a^2}{4U_0}\left[1 - exp(-\frac{2x}{l})\right] \tag{1.26}$$

Therefore, the detector response $\Delta U = U_2(\infty)$ correspond to Eq. 1.9, on condition sub terahertz non-resonant regime ($\omega\tau<1$) [1]. Eq. 1.26 can derived relation of channel characteristic length effect to photoresponse

1.3 Motivation

For terahertz applications system, we will need a compact model that describes the elementary complementary metal oxide semiconductor (CMOS) device entering the circuit However, Berkeley short channel IFGET model (BSIM) model for the current simulation program with integrated circuit emphasis (SPICE) Simulation, plasma wave transit time lager than oscillation time of the electromagnetic waves into the MOSFET, There is a limit to express the physical elements of the device operation principle in the high-frequency domain, it is not to represent the behavior of the terahertz region. In this thesis we propose a BSIM model that operates in terahertz region using the non quasi static (NQS) based analysis, and we explain how to extract the photoresponse.

1.4 Thesis overview

In this thesis, we propose a novel methodology for designing the Si-MOSFET as a non-resonant plasmonic THz detector with photoresponse characteristic in the form of DC voltage, on the basis of technology computer-aided design (TCAD), SPICE simulation platform without the rigorous hydrodynamic description of plasma-wave dynamics. The basic principles of non-resonant detection in FET are described in chapter 1.2, and the in chapter 2, we present non-quasi static simulation, and quasi-plasma two-dimensional electron gas (2DEG) modeling and the subsequent simulation results with various structural design parameters of the Si MOSFET. then describe the boundary condition of PWT

ULSAN NATIONAL INSTITUTE OF
SCIENCE AND TECHNOLOGY

and BSIM model based non-quasi-static model. Simulation results part describe the simulation results of SPICE, BSIM respectively, and the physical validity of NQS part shows that physical parameter variation is affect to photoresponse. Chapter3 is the summary and conclusion, finally chapter4 is future work.

ULSAN NATIONAL INSTITUTE OF
SCIENCE AND TECHNOLOGY

Chapter 2

Modeling and simulation of terahertz detector

2.1 Modeling terahertz detector

For accurate simulation and analysis of MOSFET operation, which can be partial differential equations of the continuity equation for the time and space to be solved numerically. This numerical method it requires a lot of calculation, which is suitable in TCAD based simulation for analysis 1 device characteristic. But that is no suitable for the SPICE simulation for fast processing speed. Thus SPICE simulation, SPICE using approximation the continuity equation over the ordinary differential equation for fast simulation. THz regime beyond MOSFET cutoff frequency SPICE, which cannot reproduce NQS effect in the channel. NQS effect is incident frequency is very faster than MOSFET channel electron density variation, delay occurs in the channel electron density. In order to solve this phenomenon, BSIM support NQS model. In this chapter we modeling non resonant plasmonic THz detector consider applied a boundary condition using two kinds of simulation program TCAD, and SPICE.

2.1.1 Quasi static and non quasi static mode

In generally, physical value analysis of the time that is two-kinds of way are exist. That is static analysis, dynamic analysis. Static analysis is the physical value not changed by time. Dynamic analysis is the physical value variation changed by time dramatically. So quasi means sub state prefix. The non quasi static means that same topology in the dynamic analysis. These theory apply to electron variation in the MOSFET channel, ac voltage induced in the gate electron modulation alongside of source and drain. But this is valid only under the MOSFET cut-off frequency, but terahertz detector operating frequency is much higher than MOSFET cut-off frequency. In this region MOSFET general equation about operation principle is not valid transit time analysis. In Fig. 2-2 show that contour plot simulation results in the TCAD frame work. It show that incident frequency is higher MOSFET channel electron variation cannot react signal variation. As shown in Fig. 2-1 the terahertz detector structure and simulation framework based on Si FET. In this simulation results show that in the low frequency regime in 6 GHz, electron modulation shape shows that electron react immediately of the signal variation, but consider high frequency regime in 600 GHz electron modulation cannot react the signal variation. As a result, low frequency regime quasi static analysis is suitable, and high frequency regime non quasi static analysis is applicable.

ULSAN NATIONAL INSTITUTE OF SCIENCE AND TECHNOLOGY

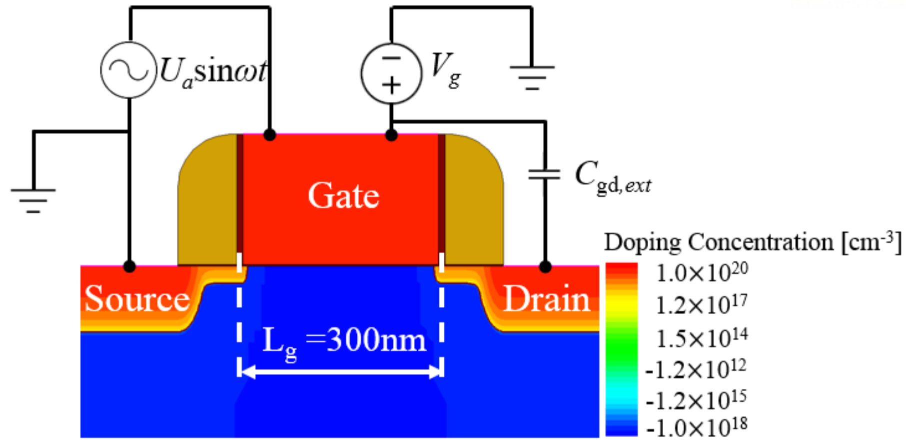

Figure 2-1. Terahertz detector structure and simulation framework based on Si FET. To the boundary condition external capacitor connected to gate and drain (L_g= 300 nm, t_{ox}= 1.1 nm, V_{th}= 0.2 V)

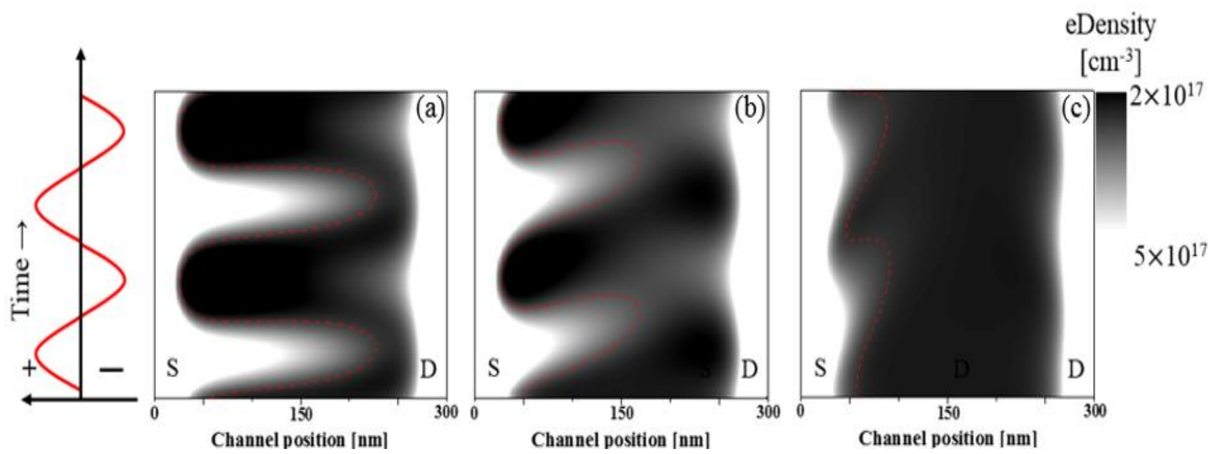

Figure 2-2. Contour plot of the channel electron density modulation along with the channel position at the same gate overdrive voltage V_g - V_{th}= 0.1 and each gate incident frequency (a) 6 GHz, (b) 60 GHz, (c) 600 GHz

And other theory is plasma wave transit time vs. oscillation period. Gate incident THz signal excited in the source and drain plasma wave is caused the each side. If the condition is fulfilled that the plasma-wave transit time τ_t^{pl} through the channel is much shorter than the oscillation period of the radiation field. For $e(U_g\text{-}U_{th})>>\eta k_B t$ (η being the ideality factor of the transport in the channel) the plasma wave transit time equation [38] :

$$\tau_t^{pl} = \sqrt{\frac{L^2 m}{e(U_g - U_{th})}} \tag{2.1}$$

U_{th} is the threshold voltage of the MOSFET, U_g is the gate voltage, L is the channel length of transistor the equation results is shown in Table. 1. For example, when gate length 300 nm, plasma wave transit time is 3.65 ps. And consider oscillation of the gate incident terahertz is shown that in the terahertz regime is the non-quasi-static simulation is suitable for simulation in Table 1.

Frequency	τ_t^{pl} (s)	Oscillation period (s)
6 GHz	3.65×10^{-12}	160×10^{-12}
7 GHz	3.65×10^{-12}	143×10^{-12}
600 GHz	3.65×10^{-12}	1.6×10^{-12}
700 GHz	3.65×10^{-12}	1.43×10^{-12}

Table 1. Calculation results of plasma wave transit time (L_g= 300 nm), oscillation period of the each frequency (6 GHz, 7 GHz, 600 GHz, 700 GHz)

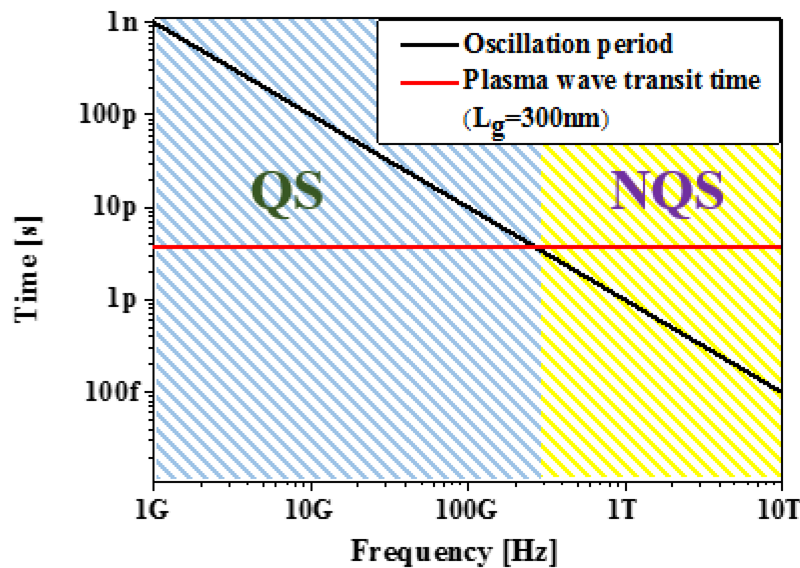

Figure 2-3. Calculation of the plasma wave transit time, oscillation period

As a result show that low frequency regime is suitable in quasi static analysis, and High frequency regime (THz regime) is non-quasi-static simulation is suitable (Fig. 2-3).

ULSAN NATIONAL INSTITUTE OF SCIENCE AND TECHNOLOGY

2.1.2 TCAD modeling (boundary condition)

From the given boundary conditions for non-resonant broadband THz detectors, the asymmetry in the channel electron distribution will be induced and thus. As shown in Fig. 2-4 shows the transient simulation of the mixed-mode TCAD [38] by adding varied external capacitance between gate and drain, because it is necessary to asymmetry environment between source and drain for extracting Δu in non-resonant THz detector based on Si MOSFET [40][41]. Since the gate-to source voltage (V_{gs}) has been applied as $U_a \sin\omega t + V_g$, the gate-to-drain voltage (V_{gd}). Our design MOSFET oxide thickness is 1.1 nm, that gate oxide capacitance is:

$$C_{ox} = \frac{\varepsilon_{ox}}{t_{ox}} \cdot W \cdot L \cong 10\text{fF} \qquad (2.2)$$

where W is the device width, 1 um, and L is the length, 300 nm. ε_{ox} is oxide permittivity 3.45×10^{-13} F/cm. As shown in Fig. 2-4, $C_{gd,ext}$ is larger than 100 times of gate oxide capacitance, AC short between gate and drain. And can be saturated to DC output voltage as gate-to-drain capacitance (C_{gd}) increases. Thus, the C_{gd} is satisfied with boundary condition in our device for detecting THz wave.

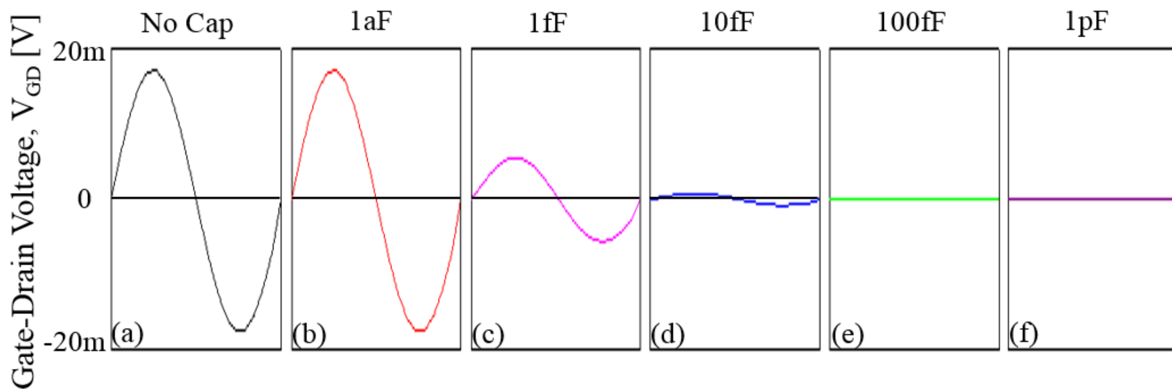

Figure 2-4. The applied asymmetric boundary condition in the transient simulation of the mixed-mode TCAD framework (Fig. 2-1) by adding varied external capacitance between gate and drain

Figure.2-5 show that the modulation of the channel 2DEG density at 0.7 THz transient simulation has been demonstrated with TCAD frame work based on the coupled Drude and continuity equation with normal electric field dependent mobility model. These contour plots of the channel 2DEG density (at t_{ox}= 1.1 nm) modulation along with the channel position at each time scale depend on the symmetric. In terms of the symmetric condition, it is equal to propagation distance at source and drain side. According to adding increasingly capacitance 1 pF in Fig. 2-5(b). As saturated asymmetric condition is

satisfied with boundary condition at C_{GD}= 1 pF.

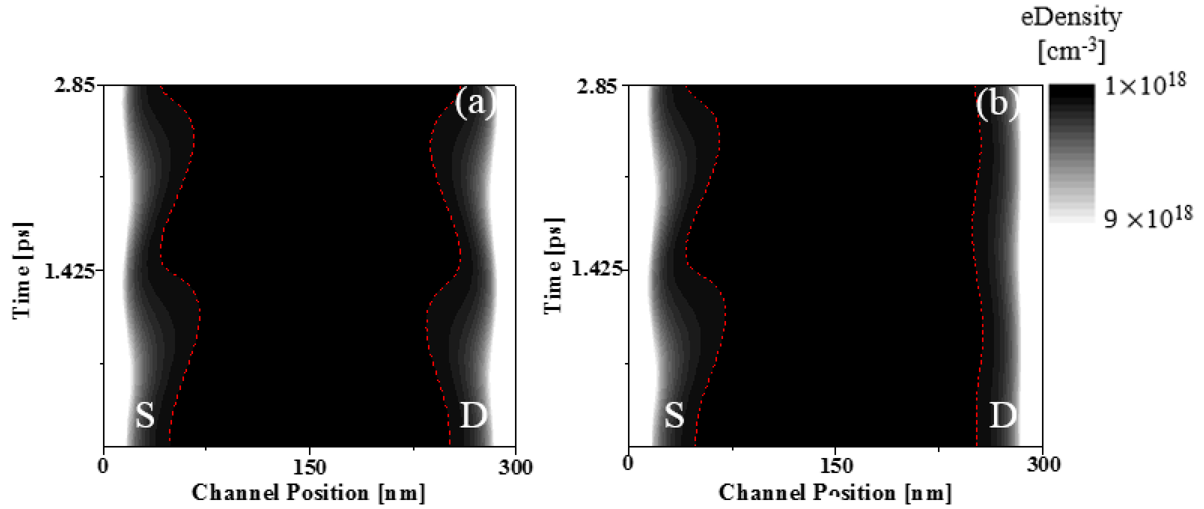

Figure 2-5. Contour plots of the channel electron density modulation along with the channel position at each time scale. The 2DEG density is modulated near source side due to incoming THz radiation with f= 0.7 THz (a) symmetry condition, (b) C_{gd}=1 pF

2.1.3 Quasi plasma 2DEG

Figure. 2-6 shows the Si MOSFET-based THz detector structure and circuit configuration where the AC voltage source represents the incoming THz wave, which induces the output DC voltage difference Δu between source and drain. For the rigorous description of plasma-wave decay and propagation in the channel region, the numerical solution of the continuity equation Eq. 1.2 and hydrodynamic Euler equation Eq. 1.1 all together with Poisson's equation is mathematically challenging owing to the high computational cost of the structural design of MOSFETs with frequency and time domains. In the non-resonant detection mode ($\omega\tau < 1$), however, the plasma waves of 2DEG cannot exist in the channel because of over damping, which means a longer propagation length than the coherent distance, and thus, this eventually give rise to the asymmetric channel electron distribution along with the channel length direction [13]. Therefore, as shown in the inset Fig. 2-7, we modeled the quasi-plasma electron box on the basis of the assumption of 'quasi-static' 2DEGplasma density for the resultant channel electron distribution with asymmetry during the exposure to THz radiation. Even though the resultant 2DEG behavior should be described by the hydrodynamic Euler equation with the convection component in the rigorous manner, the quasi-plasma 2DEG modeling has been performed on the basis of the TCAD platform [39], which does not include the hydrodynamic Euler formalism, for the efficient simulation of non-resonant broadband THz detectors by exploiting the advantage of well-established MOSFET models and the DC/AC analysis environment on TCAD. In Fig. 2-6 shows that the Contour plots of the

channel electron density modulation along with the channel position at each time scale, in this simulation results show that the quasi plasma 2DEG length is 63 nm, and 2DEG density is the average value of the electron density modulation

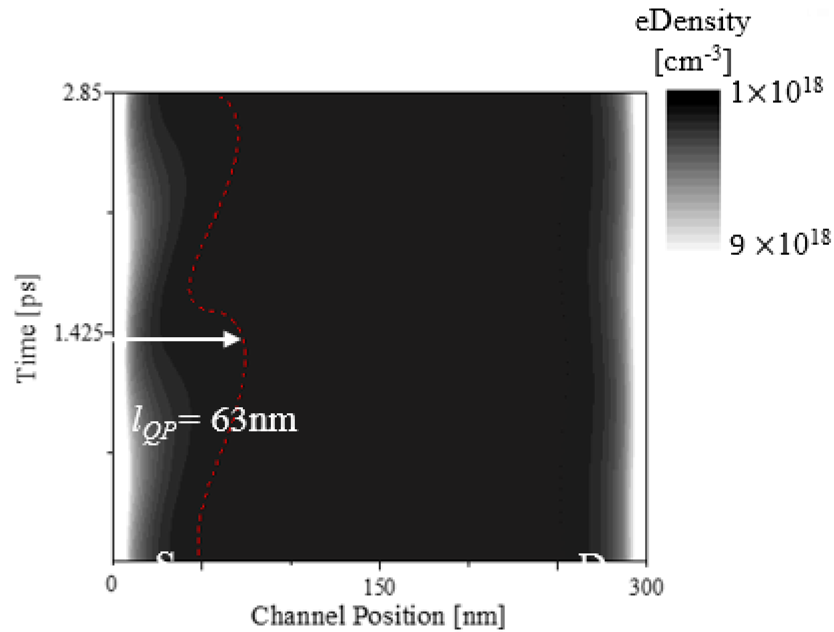

Figure 2-6. Contour plots of the channel density modulation along with the channel position

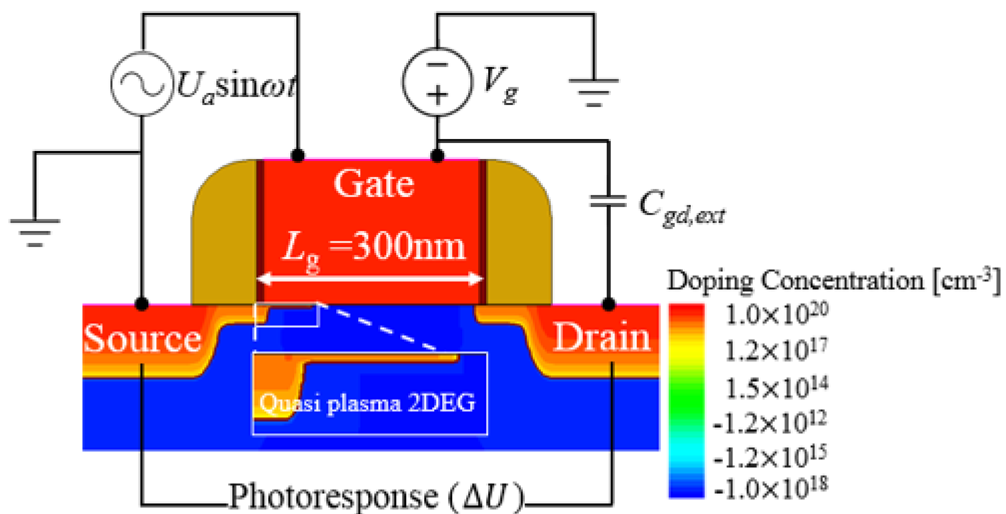

Figure 2-7. Si MOSFET-based THz detector structure and circuit configuration in TCAD simulation, Inset shows the quasi-plasma electron box as 2DEG in the channel region

In our quasi-plasma modeling under the given temperature (T= 300K) and with constant doping profiles. Quasi plasma 2DEG length is determined by, electron modulation simulation TCAD frame work and extract max length of the source side length,

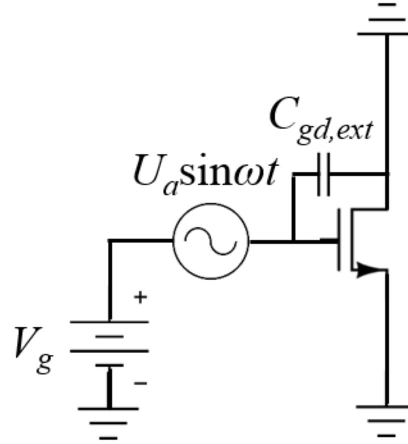

Figure 2-8. The schematic of applied asymmetric boundary condition in the transient simulation of the mixed-mode SPICE framework by adding varied external capacitance between gate and drain (L_g= 300 nm, t_{ox}= 1.1nm, V_{th}= 0.2V)

2.1.4 SPICE modeling (boundary condition)

As shown in Fig. 2-8 shows the transient simulation of the mixed-mode SPICE [38] by adding varied external capacitance between gate and drain, for asymmetry boundary condition environment between source and drain for extracting Δu in non-resonant THz detector based on Si MOSFET [40][41]. Since the gate-to source voltage (V_{gs}) has been applied as $U_a\sin\omega t + V_g$, the gate-to-drain voltage (V_{gd}) can be saturated to DC output voltage as gate-to-drain capacitance (C_{gd}) increases. Thus, the C_{gd} is satisfied with asymmetry boundary condition in out device for detecting THz wave. Our design SPICE platform MOSFET t_{ox} is 1.1 nm, that gate oxide capacitance is equal to TCAD modeling part. As shown in Fig. 2-8, $C_{gd,ext}$ is larger than 100 times of gate oxide capacitance, AC short between gate and drain. And can be saturated to DC output voltage as gate-to-drain capacitance (C_{gd}) increases. Thus, the C_{gd} is satisfied with asymmetry boundary condition in device for detecting THz wave.

ULSAN NATIONAL INSTITUTE OF
SCIENCE AND TECHNOLOGY

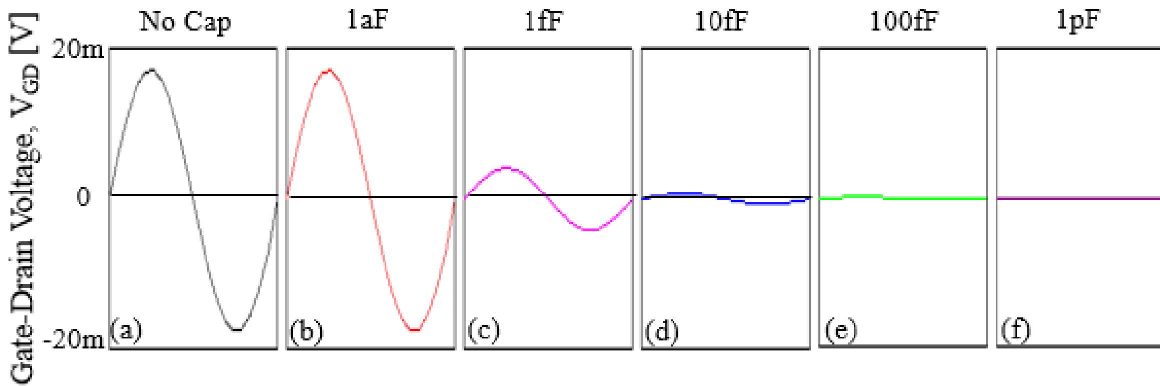

Figure 2-9. The applied asymmetric boundary condition in the transient simulation of the mixed-mode SPICE framework (Fig. 2-8) by adding varied external capacitance between gate and drain

2.1.5 SPICE modeling (non quasi static)

For exact analysis MOSFET, that can be solved continuity equation with time and space. But this topology is many calculations, simulation time. So, that is not suitable in the SPICE program. The SPICE program using the continuity equation changed to ordinary differential equation approximation. It called Quasi-static approximation. But in the High frequency regime, these tools not suitable. Because, high-frequency regime inversion layer charge response has delay compare with the incident frequency. This phenomenon is NQS effect. In the SPICE simulation same topology need to be applied. For NQS modeling other research groups using the RC ladder model (Fig. 2-10) in this model R is the MOSFET channel resistance R_{ch}, C is the MOSFET oxide capacitance. For example, modeling 300 nm NQS model, we using the 10 segments of MOSFET divided same channel length 30nm. Decreasing size of MOSFET we consider short channel effect that is the difficulty of RC ladder modeling. And all parasitic elements is substitute passive elements that is the other difficulty of the model [51]. For solution of that difficulty, BSIM3 supports the New Elmore model. Making equivalent circuit using the Elmore resistance R_{elmore}. In Fig 2-10, Elmore resistance role is the making delay of source and drain side, RC delay. That is the making charge delay in the channel to describe NQS effect. Elmore resistor is defined as:

$$R_{elmore} = \frac{L_{eff}}{elmore\left(\mu_{eff} \mathrm{W}_{\mathrm{eff}} \mathrm{Q}_{\mathrm{ch}}\right)} \tag{2.4}$$

elmore is the Elmore constant to match the lowest frequency pole , Q_{ch} is the instantaneous channel inversion charge [45]. Thus, we using the elemore resistor making the delay between the source, drain. For make the delay in the MOSFET compact model.

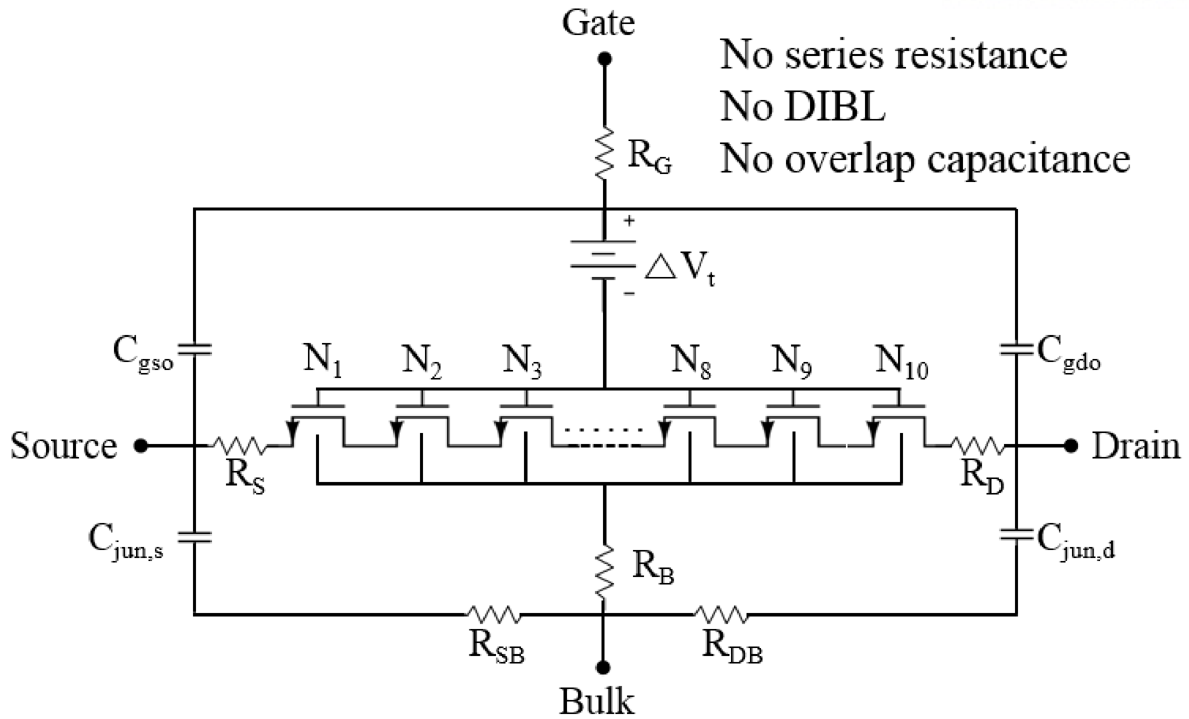

Figure 2-10. Equivalent circuit of the NQS model [43]

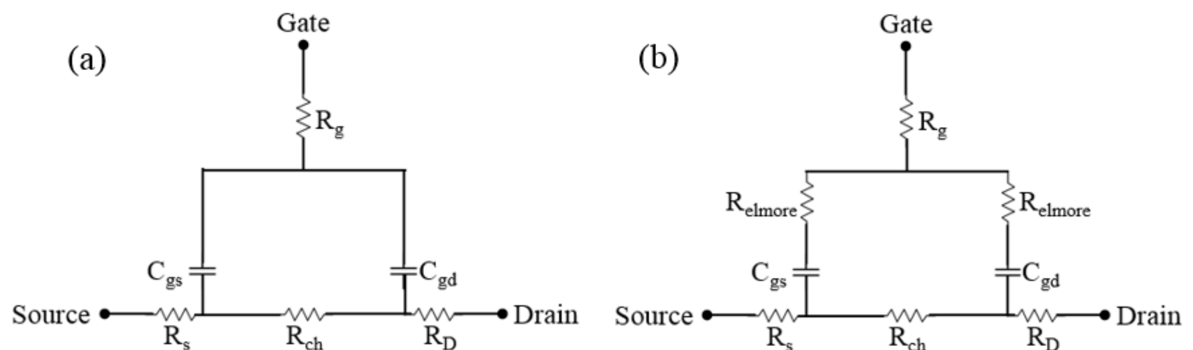

Figure 2-11. Equivalent circuit BSIM model (a) quasi-static model, (b) new Elmore equivalent model for non quasi static model [42]

In the spice modeling for compact model BSIM that transient simulation is low frequency regime is Fig. 2-10 (a) is suitable, but high frequency regime for NQS modeling the Fig. 2-10(b) is suitable the Elemore resistor is making delay, in the incident signal that cause the charge transit time delay to quasi static simulation. [45]-[48]

2.2 Simulation results of terahertz detector

2.2.1 TCAD, SPICE simulation results

In the TCAD part Fig. 2-12 shows the TCAD simulation results of ⊿u as a function of gate voltage V_g at f= 0.7 THz, U_a is the 50 mV. As we discussed in TCAD modeling part, for solution of absence hydrodynamic equation model, we using the quasi plasma 2DEG in the channel. Figure 2-12(a) shows that the without Quasi plasma 2DEG simulation results. That result shows inaccurate for THz detector operation. As shown in Fig. 2-12(b) shows that our quasi plasma modeling can successfully describe the behavior of non-resonant THz detectors in that ⊿u increases in the subthreshold region.

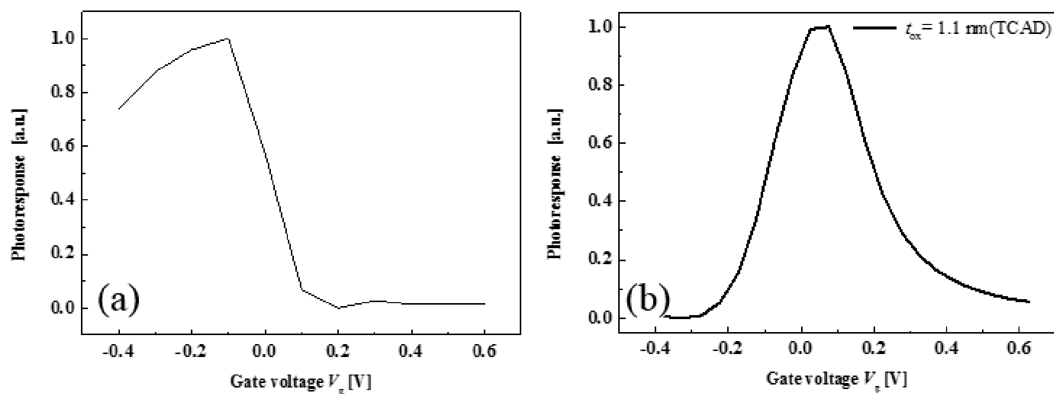

Figure 2-12. Simulation results of photoresponse in TCAD framework as a function of a gate voltage (a) Without Quasi plasma 2DEG, (b) Apply Quasi plasma 2DEG in the channel

In the SPICE framework simulation results shows that, as shown in Fig. 2-12 the THz spice model was simulated using the equivalent circuit. Incident THz radiation was modeled by applying a sinusoidal signal of amplitude U_a , representing the magnitude of the coupled radiation at the gate. The gate of the device was biased by a DC gate voltage, V_{gs}..To measure response, the sinusoidal wave seen at the drain is integrated over time to find the DC shift representing response, Δu (Fig. 2-14) Using this modeling theory we try to transient simulation in the U_a= 50 mV, f= 0.7 THz, Fig. 2-14 shows that THz response as a function of applied gate-bias voltages. Adding the load resistor of finite value creates a voltage divider circuit between the channel resistance and load [44]

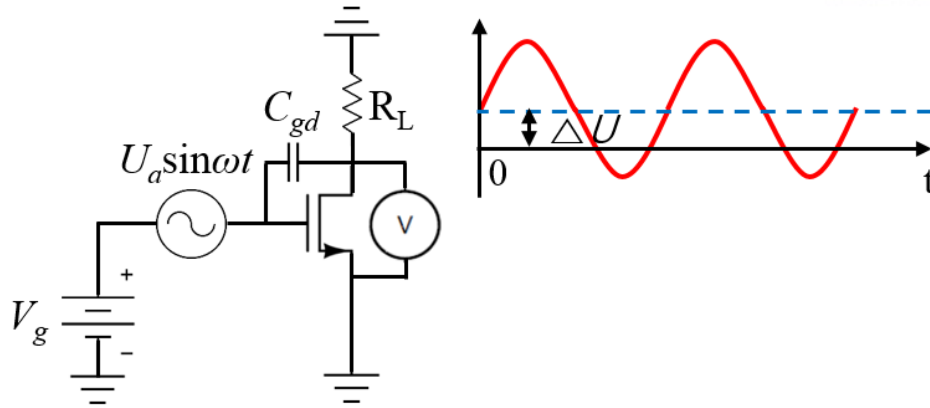

Figure 2-13. Schematic of SPICE simulation circuit, L_g= 300 nm, t_{ox}= 1.1 nm, V_{th}= 0.2 V

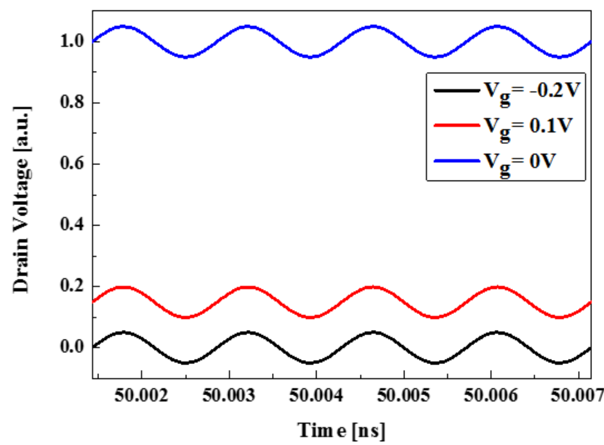

Figure 2-14. Transient simulation results of drain voltage at each gate DC voltage 0, 0.1, and -0.2V respectively

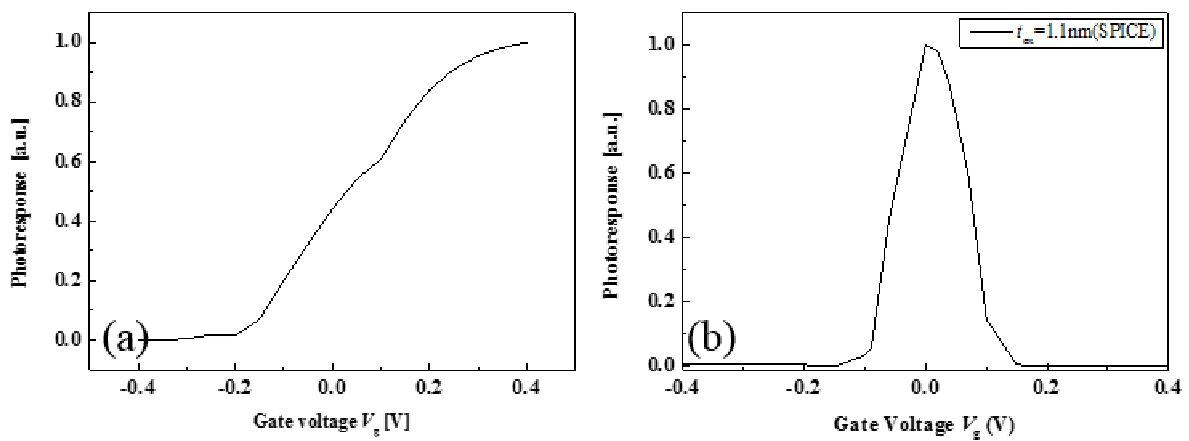

Figure 2-15. SPICE simulation results of the photoresponse by function of gate voltage (a) Quasi static model, (b) Non Quasi static model

ULSAN NATIONAL INSTITUTE OF SCIENCE AND TECHNOLOGY

2.2.2 Physical validity of our NQS model

As shown in Fig. 2-16, the electron density contour plots for extracting the Quasi-plasma 2DEG modeling by according to t_{ox}. In case of the ultra-thin gate dielectric, Electron density is sensitive as biased gate voltage. As thinner t_{ox}, electron density increases in 2DEG density modulation by improved subthreshold swing (SSW) of FET, and photoresponse enhancement [49][50].

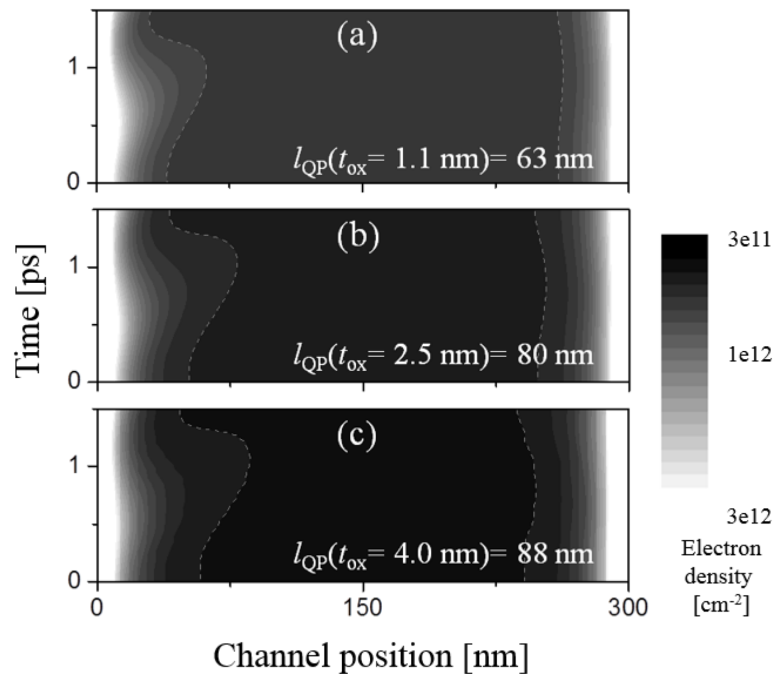

Figure 2-17. Contour plots of the channel density modulation along with the channel position at the same gate overdrive voltage V_g - V_{th}

The propagation distance from the 2DEG density simulation results decreases by reducing t_{ox}, since the modulation and propagation of a plasma-wave electron fluid ($l=s(\tau/\omega)^{0.5}$) definitely depend on the plasmon decay time $\tau=\mu m/e$ where μ is the carrier mobility, m is the effective mass of electron, the parameter τ is the quality factor. These values of can be varied by scattering, electron mobility degradation according to the decrease of t_{ox} owing to the surface roughness scattering (SRS) by the enhanced normal electric field, Therefore, it can be expected that the value of 2DEG decrease by more degraded electron mobility in thinner gate dielectric [49][50]. In Eq. 1.26 2DEG length is smaller the photoresponse is increase as a result, surface roughness scattering in the thin-oxide strong e-field affect in the channel, mobility decrease, photoresponse enhancement. And other side of Eq. 1.26 we tried to changing of MOSFET length that is affect to photoreponse (Fig. 2-19) that results shows that we successfully demonstrate the channel length is increase, photoresponse enhancement.

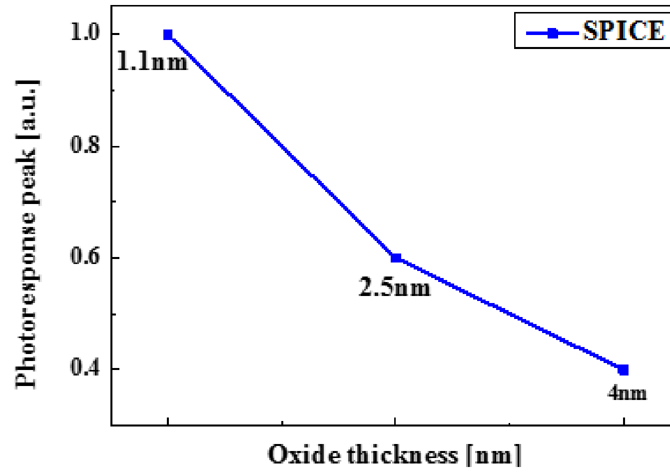

Figure 2-18. The simulation results as a function of gate voltage according to the variation t_{ox} (=1.1, 2.5, and 4 nm) spice simulation results.

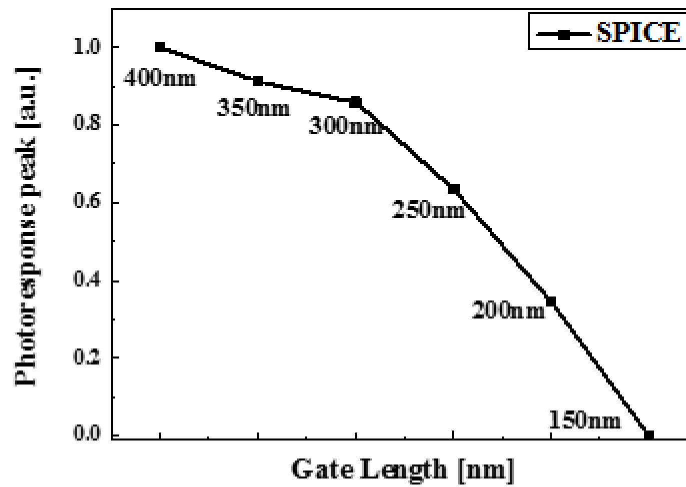

Figure 2-19. Simulation results of the SPICE photoresponse peak value of at each gate length

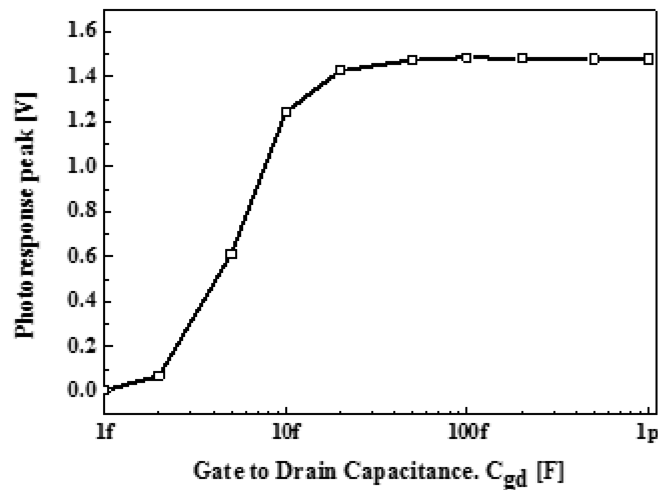

Figure 2-20. SPICE simulation results of photoresponse peak vary the gate to drain capacitance

ULSAN NATIONAL INSTITUTE OF SCIENCE AND TECHNOLOGY

As shown in Fig. 2-16 SPICE simulation results of the C_{gd} variation for apply boundary condition of our model. C_{gd} is beyond of MOSFET gate capacitance, photoresponse is increasingly dramatically, and the asymmetry boundary condition is applied in the MOSFET which is saturated of response.

2.2.3 Noise equivalent power (NEP)

For evaluate THz detector performance, noise parameter considered essential, which called noise equivalent power (NEP). Definition is, which is the incident power (sometimes per unit frequency range) producing a detector response equal to the noise voltage at the output of the device. NEP is calculated,

$$\text{NEP} = \frac{N}{R_V} \tag{2.5}$$

$$R_V = \frac{\Delta u}{P_a} \tag{2.6}$$

P_a is the actual AC power 200 nW [52]. As shown in Fig. 2-21(a) DC characteristic of each gate length of MOSFET (400 nm, 350 nm, 300 nm, 250 nm, 200 nm, and 150 nm), V_{th} is 0.18, 0.19, 0.2, 0.22, 0.228, and 0.25V respectively. In Fig. 2-21(b) shows that photorespnse results function gate voltage in each gate length, as we discussed in chapter 2.2.3 photoresponse is proportional to gate length. Figure. 2-19(c) shows that channel resistance (R_{ch}) and noise (N), these two parameter described as:

$$N = \sqrt{4kTR_{ch}} \tag{2.7}$$

$$R_{ch} = \frac{V_D}{I_D} \tag{2.8}$$

where k is the boltzmann constant, R_{ch} is channel resistance can be extracted in the MOSFET DC characteristic (Fig. 2-21(a)). NEP results show (Fig. 2-21(e)) that our NQS model as sensitive detectors of terahertz radiation.

ULSAN NATIONAL INSTITUTE OF SCIENCE AND TECHNOLOGY

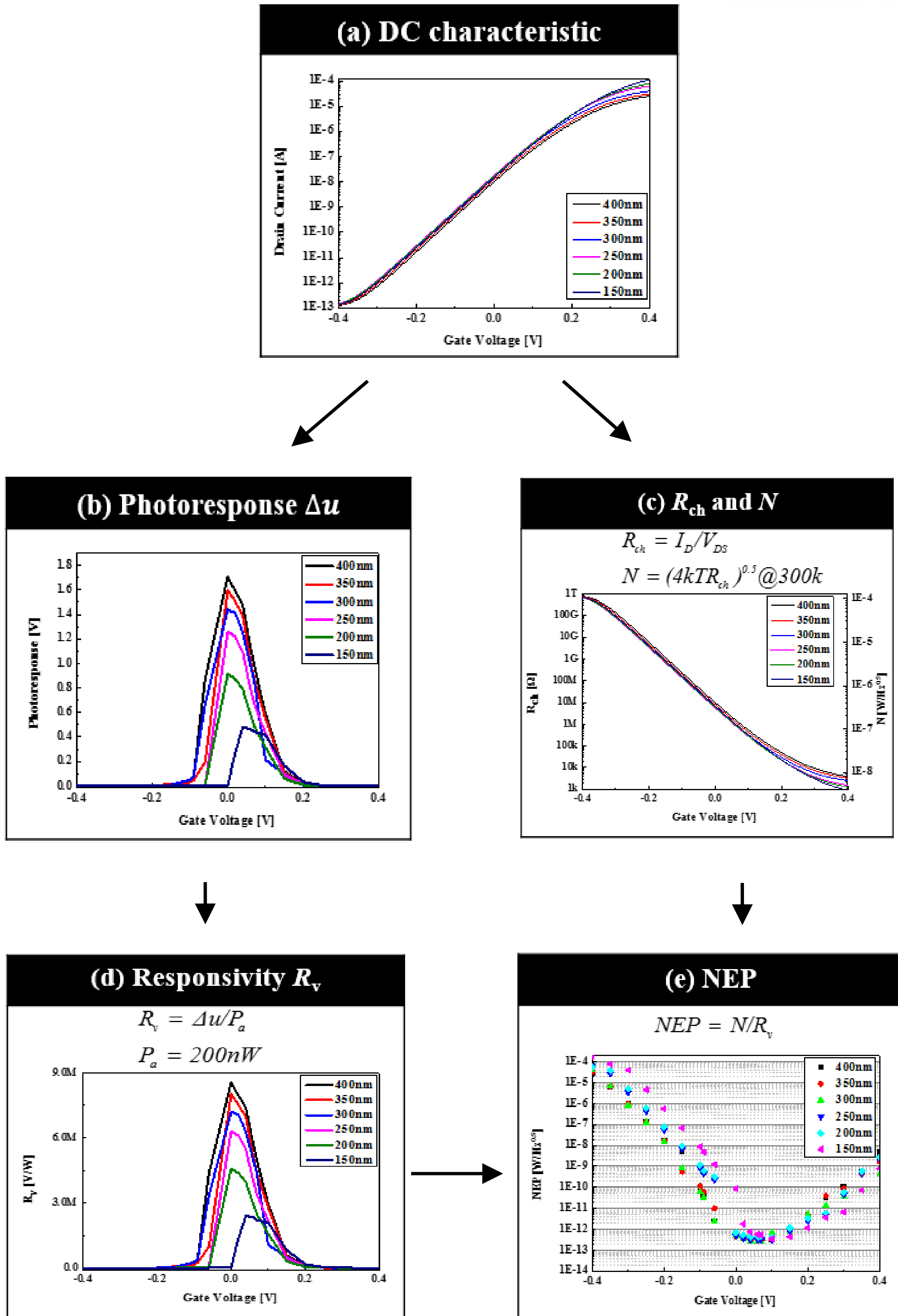

Figure 2-21. Full protocol for determining R_v and NEP

ULSAN NATIONAL INSTITUTE OF
SCIENCE AND TECHNOLOGY

Chapter 3

Summary and conclusion

In this thesis, I have reviewed the present of state-of-the-art in terahertz detectors, and established benchmarks for competitive performances, we have discussed the operation of plasma wave terahertz devices models of terahertz response based upon existing theory. In chapter1. We discussed THz, application, detector theory, in chapter2 we are discussed modeling and simulation method about the TCAD and the SPICE. Terahertz frequency regime is the beyond the MOSFET cut-off frequency, election variation cannot react THz radiation signal. And other theory we compare plasma wave transit time and oscillation. Oscillation period smaller than plasma wave transit time we need to non-quasi-static analysis is needed. The solution of the non-quasi-static modeling we are using the quasi-plasma 2DEG in TCAD platform, SPICE modeling use new Elmore model for non-quasi-static modeling. And describe the boundary condition. For conventional operate to THz detector boundary condition is essential thing, we using the capacitor between gate and drain. Lager capacitor (1 pF) is AC short between the gate and drain. In lager capacitor is the attenuation of the drain side signal that makes the ac short the drain side, and charge asymmetry in the source and drain. In the TCAD platform we using the external capacitor, SPICE simulation platform we using the BSIM intrinsic parameter set to lager cap for ac short gate and drain.

Simulation results part show that, using the transient simulation in mixed mode signal. We are extracted the photoresponse successfully. In the Eq. 1.26 shows that photoresponse peak value occurred in the subthreshold region we see the simulation results the peak value occurred in the sub-threshold regime. And photoresponse enhancement method for modeling effectiveness. Changing the physical of the MOSFET (thin-oxide, gate length) that results show the following Eq. 1.26

We modeled plasmonic THz detector in SPICE with NQS model. This SPICE modeling can be applied as a future work.

ULSAN NATIONAL INSTITUTE OF SCIENCE AND TECHNOLOGY

Chapter 4

Future Work

The purpose of the BSIM modeling is to the circuit simulation through a reliable model. Fig4.1 shows that the THz chip board for real time imaging. The THz chip board is consist of the 2×200 array of the THz detector. That each detector react terahertz wave, DC voltage output is happened than the output connected by multiplexer and dc amp connected. That the data is transmission to system, that is able to real time imaging.

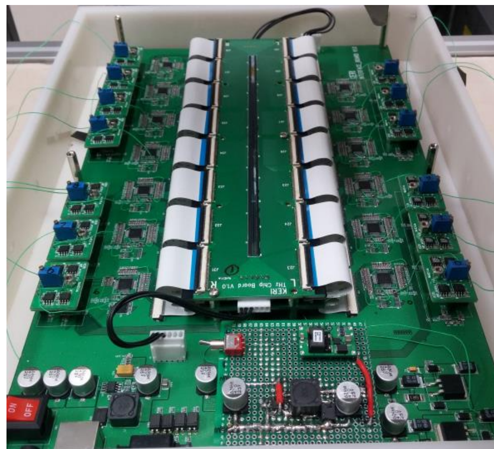

Figure 4-1. Terahertz chip board

The block diagram terahertz chip board is cannot operate all of the terahertz as the same time. We using the de-multiplexer to select the on/off device. Multiplexer output is the DC voltage connect the MOSFET gate. So mixed signal is incident the detector that dc output is passing the multiplexer. And passing the dc amp. Actually, the whole system is the simulation able. It is able to cost, time effective development is available. Future work is apply to THz detector compact model in the simulation we can predict the response of the whole system and the, design concept is optimized.

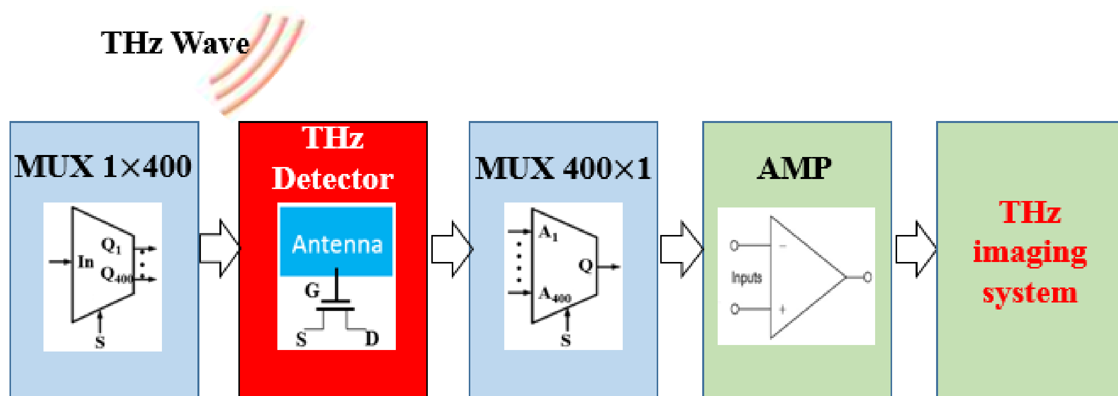

Figure 4-2. Block diagram of the terahertz chip board

ULSAN NATIONAL INSTITUTE OF
SCIENCE AND TECHNOLOGY

REFERENCES

1. Knap, W., Dyakonov, M., Coquillat, D., Teppe, F., Dyakonova, N., Łusakowski, J., ... & Otsuji, T. (2009). Field effect transistors for terahertz detection: physics and first imaging applications. Journal of Infrared, Millimeter, and Terahertz Waves, 30(12), 1319-1337.

2. Ryzhii, V., Khmyrova, I., & Shur, M. (2002). Terahertz photomixing in quantum well structures using resonant excitation of plasma oscillations. Journal of applied physics, 91(4), 1875-1881.

3. Nishimura, T., Magome, N., Khmyrova, I., Suemitsu, T., Knap, W., & Otsuji, T. (2009). Analysis of fringing effect on resonant plasma frequency in plasma wave devices. Japanese Journal of Applied Physics, 48(4S), 04C096.

4. Nishimura, T., Magome, N., & Otsuji, T. (2010). An intensity modulator for terahertz electromagnetic waves utilizing two-dimensional plasmon resonance in a dual-grating-gate high-electron-mobility transistor. Japanese Journal of Applied Physics, 49(5R), 054301.

5. Knap, W., Teppe, F., Dyakonova, N., Coquillat, D., & Łusakowski, J. (2008). Plasma wave oscillations in nanometer field effect transistors for terahertz detection and emission. Journal of Physics: Condensed Matter, 20(38), 384205.

6. Knap, W., Deng, Y., Rumyantsev, S., Lü, J. Q., Shur, M. S., Saylor, C. A., & Brunel, L. C. (2002). Resonant detection of subterahertz radiation by plasma waves in a submicron field-effect transistor. Applied physics letters, 80(18), 3433-3435.

7. Peralta, X. G., Allen, S. J., Wanke, M. C., Harff, N. E., Simmons, J. A., Lilly, M. P., ... & Eisenstein, J. P. (2002). Terahertz photoconductivity and plasmon modes in double-quantum-well field-effect transistors. Applied Physics Letters, 81(9), 1627-1629.

8. Morozov, S. V., Marem'yanin, K. V., Kuritsin, D. I., Sergeev, S. M., Antonov, A. V., Gavrilenko, L. V., ... & Gavrilenko, V. I. (2009, November). Relaxation of THz impurity photoconductivity in GaAs/InGaAsP and Ge/GeSi quantum well heterostructures. In Journal of Physics: Conference Series (Vol. 193, No. 1, p. 012087). IOP Publishing.

9. Otsuji, T., Hanabe, M., & Ogawara, O. (2004). Terahertz plasma wave resonance of two-dimensional electrons in InGaP⁄ InGaAs⁄ GaAs high-electron-mobility transistors. Applied physics letters, 85(11), 2119-2121.

10. El Fatimy, A., Teppe, F., Dyakonova, N., Knap, W., Seliuta, D., Valušis, G., ... & Rumyantsev, S. (2006). Resonant and voltage-tunable terahertz detection in InGaAs⁄ InP nanometer transistors. Applied physics letters, 89(13), 131926.

11. Knap, W., Kachorovskii, V., Deng, Y., Rumyantsev, S., Lü, J. Q., Gaska, R., ... & Brunel, L. C. (2002). Nonresonant detection of terahertz radiation in field effect transistors. Journal of Applied Physics, 91(11), 9346-9353.

12. Dyakonov, M., & Shur, M. (1993). Shallow water analogy for a ballistic field effect transistor: New mechanism of plasma wave generation by dc current. Physical review letters, 71(15), 2465.

13. Dyakonov, M., & Shur, M. (1996). Detection, mixing, and frequency multiplication of terahertz radiation by two-dimensional electronic fluid. Electron Devices, IEEE Transactions on, 43(3), 380-387.

14. Lee, A. W., & Hu, Q. (2005). Real-time, continuous-wave terahertz imaging by use of a microbolometer focal-plane array. Optics letters, 30(19), 2563-2565.

15. Lee, A. W., Williams, B. S., Kumar, S., Hu, Q., & Reno, J. L. (2006). Real-time imaging using a 4.3-THz quantum cascade laser and a 320/spl times/240 microbolometer focal-plane array. Photonics Technology Letters, IEEE, 18(13), 1415-1417.

16. Ojefors, E., Pfeiffer, U. R., Lisauskas, A., & Roskos, H. G. (2009). A 0.65 THz focal-plane array in a quarter-micron CMOS process technology. Solid-State Circuits, IEEE Journal of, 44(7), 1968-1976.

17. Oda, N. (2010). Uncooled bolometer-type Terahertz focal plane array and camera for real-time imaging. Comptes Rendus Physique, 11(7), 496-509.

18. Dem'yanenko, M. A., Esaev, D. G., Knyazev, B. A., Kulipanov, G. N., & Vinokurov, N. A. (2008). Imaging with a 90frames⁄s microbolometer focal plane array and high-power terahertz free electron laser. Applied physics letters, 92(13), 131116.

19. Pfeiffer, U. R., & Ojefors, E. (2008, September). A 600-GHz CMOS focal-plane array for terahertz imaging applications. In Solid-State Circuits Conference, 2008. ESSCIRC 2008. 34th European (pp. 110-113). IEEE.

20. Lisauskas, A., Glaab, D., Roskos, H. G., Oejefors, E., & Pfeiffer, U. R. (2009, February). Terahertz imaging with Si MOSFET focal-plane arrays. In SPIE OPTO: Integrated Optoelectronic Devices (pp. 72150J-72150J). International Society for Optics and Photonics.

21. Rogalski, A., & Sizov, F. (2011). Terahertz detectors and focal plane arrays. Opto-electronics review, 19(3), 346-404.

22. Pickwell, E., & Wallace, V. P. (2006). Biomedical applications of terahertz technology. Journal of Physics D: Applied Physics, 39(17), R301.

23. Lee, Y. S. (2009). Principles of Terahertz Science and Technology: Proceedings of the International Conference, Held in Mainz, Germany, June 5-9, 1979 (Vol. 170). Springer.

24. IEEE 802.15 WPANTM Terahertz Interest Group. http://www.ieee802.org/15/pub/IGthz.html

25. Nagatsuma, T., & Hirata, A. (2004). 10-Gbit/s wireless link technology using the 120-GHz band. NTT Technical Review, 2(11), 58-62.

26. Nagatsuma, T., Hirata, A., Kukutsu, N., & Kado, Y. (2007, October). Multiplexed transmission of uncompressed HDTV signals using 120-GHz-band millimeter-wave wireless link. In Microwave Photonics, 2007 IEEE International Topical Meeting on (pp. 237-240). IEEE.

27. Yamaguchi, R., Hirata, A., Kosugi, T., Takahashi, H., Kukutsu, N., Nagatsuma, T., ... & Nakayama, T. (2008). 10-Gbit/s MMIC wireless link exceeding 800 meters. In 2008 IEEE Radio and Wireless Symposium (pp. 695-698).

ULSAN NATIONAL INSTITUTE OF SCIENCE AND TECHNOLOGY

28. Tauk, R., Teppe, F., Boubanga, S., Coquillat, D., Knap, W., Meziani, Y. M., ... & Shur, M. S. (2006). Plasma wave detection of terahertz radiation by silicon field effects transistors: Responsivity and noise equivalent power. Applied Physics Letters, 89(25), 253511-253511.

29. Knap, W., Teppe, F., Meziani, Y., Dyakonova, N., Lusakowski, J., Boeuf, F., ... & Shur, M. S. (2004). Plasma wave detection of sub-terahertz and terahertz radiation by silicon field-effect transistors. Applied Physics Letters, 85(4), 675-677.

30. Stillman, W., Veksler, D., Elkhatib, T. A., Salama, K., Guarin, F., & Shur, M. S. (2008). Sub-terahertz testing of silicon MOSFET. Electronics Letters, 44(22), 1325-1327.

31. Pala, N., Teppe, F., Veksler, D., Deng, Y., Shur, M. S., & Gaska, R. (2005). Nonresonant detection of terahertz radiation by silicon-on-insulator MOSFETs. Electronics Letters, 41(7), 447-449.

32. Deng, Y., & Shur, M. S. (2003). Electron mobility and terahertz detection using silicon MOSFETs. Solid-State Electronics, 47(9), 1559-1563.

33. Łusakowski, J. (2007). Nanometer transistors for emission and detection of THz radiation. Thin solid films, 515(10), 4327-4332.

34. Shur, M. S., & Ryzhii, V. (2003). Plasma wave electronics. International journal of high speed electronics and systems, 13(02), 575-600.

35. Gutin, A., Ytterdal, T., Kachorovskii, V., Muraviev, A., & Shur, M. (2013). THz spice for modeling detectors and nonquadratic response at large input signal. Sensors Journal, IEEE, 13(1), 55-62.

36. Gutin, A., Nahar, S., Hella, M., & Shur, M. (2013). Modeling terahertz plasmonic si fets with spice.

37. Gutin, A., Muraviev, A., Shur, M., Kachorovskii, V., & Ytterdal, T. (2012). Large signal analytical and SPICE model of THz plasmonic FET. In Lester Eastman Conference on High Performance Devices (LEC) (pp. 1-5).

38. Lisauskas, A., Pfeiffer, U., Öjefors, E., Bolìvar, P. H., Glaab, D., & Roskos, H. G. (2009). Rational design of high-responsivity detectors of terahertz radiation based on distributed self-mixing in silicon field-effect transistors. Journal of Applied Physics, 105(11), 114511.

39. Synopsys Sentaurus Device 3-D User Guide Version D-2010.03 (2010)

40. Ryu, M. W., Sung-Ho, K. I. M., Hwang, H. C., Kibog, P. A. R. K., & Kim, K. R. (2013). Plasmonic terahertz wave detectors based on silicon Field-effect transistors. IEICE Transactions on Electronics, 96(5), 649-654.

41. Ryu, M. W., Park, K., Park, W. K., Han, S. T., & Kim, K. R. (2013, June). Plasmonic terahertz wave detector based on silicon field-effect transistors with asymmetric source and drain structures. In Device Research Conference (DRC), 2013 71st Annual (pp. 97-98). IEEE.

42. Cheng, Y., & Hu, C. (1999). MOSFET modeling & BSIM3 user's guide. Springer.

ULSAN NATIONAL INSTITUTE OF SCIENCE AND TECHNOLOGY

43. Scholten, A. J., Tiemeijer, L. F., De Vreede, P. W. H., & Klaassen, D. B. M. (1999). A Large Signal N on-Quasi-Static MOS Model for RF Circuit Simulation.

44. Stillman, W., Shur, M. S., Veksler, D., Rumyantsev, S., & Guarin, F. (2007). Device loading effects on nonresonant detection of terahertz radiation by silicon MOSFETs. Electronics letters, 43(7), 422-423.

45. Chan, M., Hui, K. Y., Hu, C., & Ko, P. K. (1998). A robust and physical BSIM3 non-quasi-static transient and AC small-signal model for circuit simulation. Electron Devices, IEEE Transactions on, 45(4), 834-841.

46. Elmore, W. C. (1948). The transient response of damped linear networks with particular regard to wideband amplifiers. Journal of applied physics, 19(1), 55-63.

47. Pillage, L. T., & Rohrer, R. A. (1990). Asymptotic waveform evaluation for timing analysis. Computer-Aided Design of Integrated Circuits and Systems, IEEE Transactions on, 9(4), 352-366.

48. Pesic, T. V., & Jankovic, N. D. (2005). A compact nonquasi-static MOSFET model based on the equivalent nonlinear transmission line. Computer-Aided Design of Integrated Circuits and Systems, IEEE Transactions on, 24(10), 1550-1561.

49. Ryu, M. W., Lee, J. S., & Kim, K. R. (2014, August). Physical modeling and analysis for performance enhancement of nanoscale silicon field-effect transistor-based plasmonic terahertz detector. In Nanotechnology (IEEE-NANO), 2014 IEEE 14th International Conference on (pp. 971-974). IEEE.

50. Ryu, M. W., Lee, J. S., & Kim, K. R. (2014, August). Physical modeling and analysis for performance enhancement of nanoscale silicon field-effect transistor-based plasmonic terahertz detector. In Nanotechnology (IEEE-NANO), 2014 IEEE 14th International Conference on (pp. 971-974). IEEE.

51. Pfeiffer, U., Oejefors, E., Roskos, H. G., & Lisauskas, A. (2013). *U.S. Patent No. 8,547,158*. Washington, DC: U.S. Patent and Trademark Office.

52. Tauk, R., Teppe, F., Boubanga, S., Coquillat, D., Knap, W., Meziani, Y. M., ... & Shur, M. S. (2006). Plasma wave detection of terahertz radiation by silicon field effects transistors: Responsivity and noise equivalent power. *Applied Physics Letters*, *89*(25), 253511-253511.

53. Knap, W., & Dyakonov, M. I. (2013). Field effect transistors for terahertz applications. *D. Saeedkia, Handbook of terahertz technology for imaging, sensing and communications, Cambridge, Woodhead Publishing*, 121-155.

54. Dyakonov, M. I. (2010). Generation and detection of Terahertz radiation by field effect transistors. *Comptes Rendus Physique*, *11*(7), 413-420.

.